Article

Cell Reports

Topological Regulation of Synaptic AMPA Receptor Expression by the RNA-Binding Protein CPEB3

Graphical Abstract

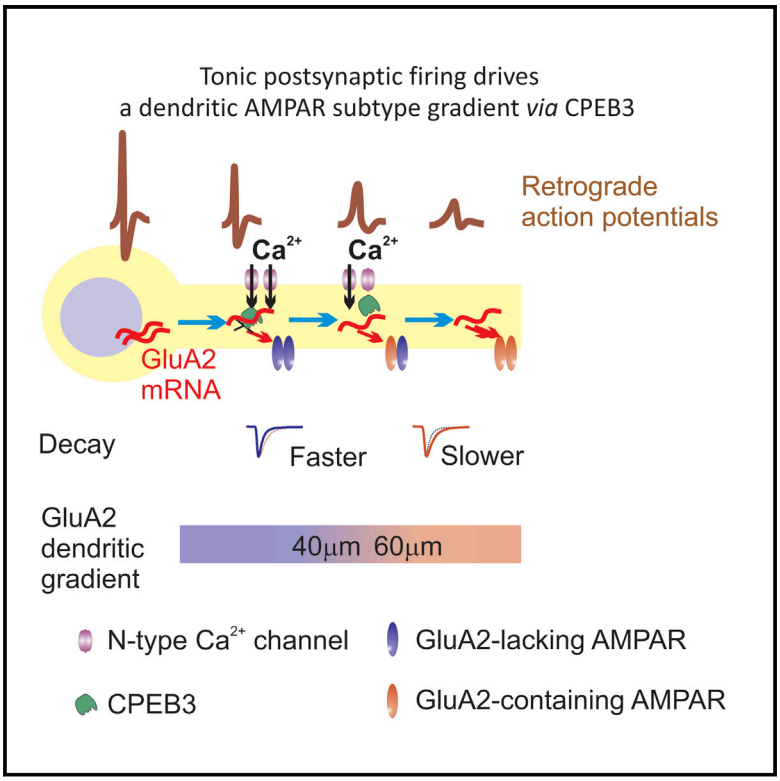

Highlights

- Synaptic GluA2-containing AMPA receptors increase along dendrites of stellate cells
- Postsynaptic action potentials and graded Ca^{2+} entry drive the GluA2 gradient
- Action potential firing activates PKC and elevates CPEB3 expression
- Elevated CPEB3 levels at proximal dendrites suppress GluA2 protein synthesis

Authors

Iaroslav Savtchouk, Lu Sun, Crhistian L. Bender, Qian Yang, Gábor Szabó, Sonia Gasparini, Siqiong June Liu

Correspondence

sliu@lsuhsc.edu

In Brief

Savtchouk et al. show there is a dendritic gradient in the expression of the GluA2 subunit in synaptic AMPA receptors. The gradient is maintained by tonic postsynaptic firing, which controls the expression of CPEB3, a translational regulator. The postsynaptic AMPA receptor gradient optimizes information processing within a cerebellar circuit.

Savtchouk et al., 2016, Cell Reports *17*, 86–103
September 27, 2016
http://dx.doi.org/10.1016/j.celrep.2016.08.094

OPEN ACCESS
CellPress

Cell Reports
Article

Topological Regulation of Synaptic AMPA Receptor Expression by the RNA-Binding Protein CPEB3

Iaroslav Savtchouk,[1,2,5] Lu Sun,[1,2,5] Crhistian L. Bender,[1,5] Qian Yang,[1,5] Gábor Szabó,[4] Sonia Gasparini,[1,3] and Siqiong June Liu[1,2,6,*]

[1]Department of Cell Biology and Anatomy, LSU Health Sciences Center, New Orleans, LA 70112, USA
[2]Department of Biology, Penn State University, State College, PA 16802, USA
[3]Neuroscience Center of Excellence, LSU Health Sciences Center, New Orleans, LA 70112, USA
[4]Laboratory of Molecular Biology and Genetics, Institute of Experimental Medicine, 1450 Budapest, Hungary
[5]Co-first author
[6]Lead Contact
*Correspondence: sliu@lsuhsc.edu
http://dx.doi.org/10.1016/j.celrep.2016.08.094

SUMMARY

Synaptic receptors gate the neuronal response to incoming signals, but they are not homogeneously distributed on dendrites. A spatially defined receptor distribution can preferentially amplify certain synaptic inputs, resize receptive fields of neurons, and optimize information processing within a neuronal circuit. Thus, a longstanding question is how the spatial organization of synaptic receptors is achieved. Here, we find that action potentials provide local signals that influence the distribution of synaptic AMPA receptors along dendrites in mouse cerebellar stellate cells. Graded dendritic depolarizations elevate CPEB3 protein at proximal dendrites, where we suggest that CPEB3 binds to GluA2 mRNA, suppressing GluA2 protein synthesis leading to a distance-dependent increase in synaptic GluA2 AMPARs. The activity-induced expression of CPEB3 requires increased Ca^{2+} and PKC activation. Our results suggest a cell-autonomous mechanism where sustained postsynaptic firing drives graded local protein synthesis, thus directing the spatial organization of synaptic AMPARs.

INTRODUCTION

Dendrites are the receptive zone for incoming signals onto a neuron, and they are strategically positioned to control diverse features of synaptic activity. Synaptic receptors are a crucial determinant of the postsynaptic response, but they are not homogeneously distributed on dendrites (Gardner et al., 2001; Magee and Cook, 2000; Major et al., 2008; Nicholson et al., 2006; Pettit et al., 1997; Stricker et al., 1996; Tóth and McBain, 1998). A spatially defined receptor distribution can preferentially amplify certain synaptic inputs, resize the receptive fields of neurons, and thereby optimize information processing within a neuronal circuit. This underlies the critical need to understand how the spatial organization of synapses on individual dendrites is achieved and maintained. Growing evidence supports the idea that dendrites integrate both the electrical and biochemical signals that are initiated by somatic action potentials (APs) and synaptic inputs (Häusser et al., 2000; Helmchen, 2007; Magee and Johnston, 2005). Somatic spikes can passively spread or actively travel backward in dendrites toward postsynaptic sites, and they elevate intracellular Ca^{2+} levels by depolarizing dendritic segments. Here we have tested the hypothesis that sustained postsynaptic firing controls the pattern of synaptic glutamate receptor subunit expression, and we have identified the local cellular process that converts electrical signals into a spatially confined receptor distribution.

AMPA-type glutamate receptors (AMPARs) mediate excitatory synaptic transmission in the CNS and are composed of four subunits (GluA1–4). Receptors that lack the GluA2 subunit display a number of distinct features, including a large channel conductance, rapid kinetics, and high Ca^{2+} permeability (Cull-Candy et al., 2006). They also exhibit a characteristic facilitation due to an activity-dependent polyamine unblock that occurs during a train of synaptic activity and that enhances the ability of excitatory postsynaptic potentials to evoke APs (Rozov and Burnashev, 1999; Savtchouk and Liu, 2011). GluA2 expression in neurons varies considerably with low GluA2 levels in a wide variety of neurons that display tonic activity, such as olfactory neurons, glutamatergic neurons in the lateral habenula, neostriatal cholinergic interneurons, auditory neurons in the deep cerebellar nucleus (DCN), and GABAergic interneurons in several brain regions (Blakemore et al., 2006; Li et al., 2011; Liu and Cull-Candy, 2000; Maroteaux and Mameli, 2012; Samoilova et al., 1999). These Ca-permeable AMPARs play a critical role in the induction of NMDAR-independent synaptic plasticity, modulation of membrane excitability, and long-range gamma oscillations (Liu and Zukin, 2007). Pyramidal neurons normally express GluA2-containing receptors, but they switch to Ca-permeable, GluA2-lacking receptors after periods of hyperexcitability, such as seizure or ischemia, and this leads to neuronal death (Liu et al., 2004; Noh et al., 2005). This suggests that one mechanism that could suppress GluA2 expression and promote the expression of synaptic Ca-permeable AMPARs could be sustained somatic AP firing.

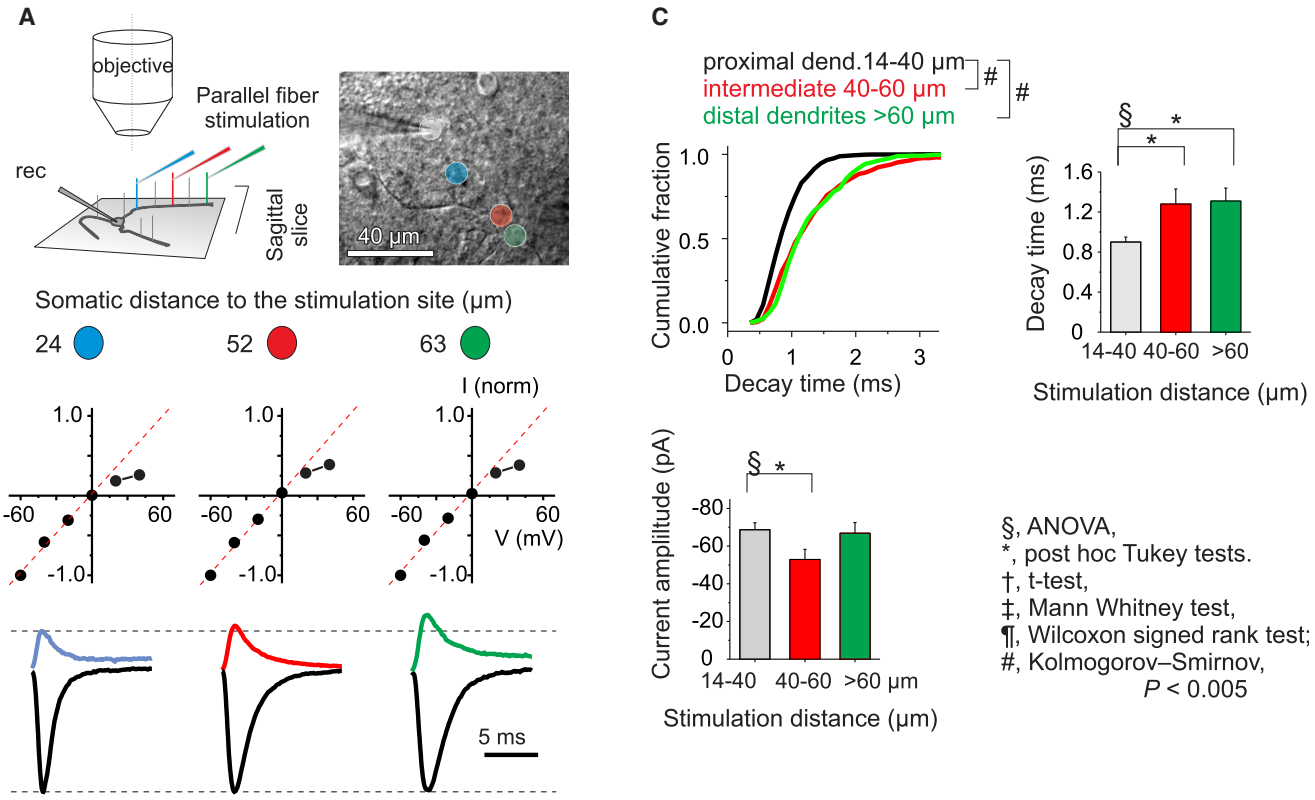

(legend on next page)

Cerebellar stellate cells display spiking activity in the absence of synaptic input, and somatic APs passively spread within the dendrites, thus elevating Ca^{2+} levels in proximal, but not distal, dendrites (Myoga et al., 2009). Excitatory synaptic transmission onto GABAergic stellate cells is largely mediated by GluA2-lacking, Ca-permeable AMPARs, but also by some GluA2-containing receptors (Liu and Cull-Candy, 2002). The difference in the excitatory postsynaptic current (EPSC) waveforms between these two AMPAR subtypes markedly alters the ability of a synaptic response to evoke an AP (Savtchouk and Liu, 2011).

Although presynaptic activity-dependent homeostasis of postsynaptic receptor expression has been studied extensively, whether postsynaptic firing influences the subunit composition pattern of synaptic AMPARs is unknown. We propose that the change in AMPAR subunit expression along dendrites relies on a graded cellular signal, which locally influences synaptic AMPAR subunit synthesis or trafficking. A transcription-dependent regulation of synaptic AMPARs by postsynaptic firing, which has been described in cortical and CA1 pyramidal neurons (Goold and Nicoll, 2010; Ibata et al., 2008) and which is controlled by nuclear localized signals, is an unlikely mechanism for generating a dendritic AMPAR subunit gradient. In contrast, cytoplasmic polyadenylation element-binding protein 3 (CPEB3), an RNA-binding protein that interacts with GluA2 mRNA and controls GluA2 synthesis, is a promising candidate (Huang et al., 2006; Theis et al., 2003; Vogler et al., 2009). Given that both the expression level and activity of CPEB3 can be altered by neuronal activity (Pavlopoulos et al., 2011; Wang and Huang, 2012), a cellular process involving dendritic CPEB3 and the local control of GluA2 synthesis may be sufficient to establish a synaptic GluA2 gradient along dendrites, a form of topostatic plasticity that homeostatically controls the spatial (or topological) distribution of AMPAR subtypes.

Here we examined the distributions of AMPAR subtypes along the dendrites of mouse cerebellar stellate cells, and we determined the impact of somatic AP activity on the spatial distribution of synaptic AMPARs. We found that the synaptic AMPAR subtype switches from GluA2 lacking to GluA2 containing as the distance of the synapses along the dendrites increases. This GluA2 gradient is driven by postsynaptic APs and requires Ca^{2+} entry at proximal dendrites and protein synthesis at distal dendrites. The depolarization-evoked Ca^{2+} rise activates protein kinase C (PKC) and elevates CPEB3 expression at proximal dendrites, where we propose that CPEB3 binds to GluA2 mRNA and suppresses GluA2 protein synthesis. This leads to a distance-dependent increase in synaptic GluA2-containing AMPARs along dendrites. Our results reveal a function for postsynaptic spiking activity in spatially defining the distribution of synaptic receptors and synaptic integration, highlighting the importance of CPEB3 expression in translating dendritic depolarization into differing expression patterns of synaptic AMPAR subtypes.

RESULTS

Distance-Dependent Distribution of Synaptic AMPAR Subtypes along Dendrites

We took advantage of a unique anatomic feature of the cerebellar cortex, in which dendrites of stellate cells lie within the sagittal plane and the excitatory inputs, parallel fiber axons, extend perpendicular to the dendritic plane. Thus, in sagittal slices the position of a stimulating electrode evokes synaptic currents in a stellate cell at a point that corresponds to the dendritic site of parallel fiber innervation (Figure 1A). This approach was used previously to map short-term plasticity along stellate cell dendrites (Abrahamsson et al., 2012). We examined whether synaptic AMPAR subtypes are differentially distributed along the dendrites of cerebellar stellate cells using three independent experimental approaches.

First, to determine AMPA subunit composition, we included spermine in the patch electrode and measured synaptic currents

Figure 1. Distance-Dependent Distribution of Synaptic AMPAR Subtypes along Dendrites

(A) Left: schematic showing that parallel fibers (vertical lines) extend orthogonally to the sagittal plane of stellate cell dendrites. The position of a stimulation electrode in a sagittal slice closely correlates with the location of a PF-stellate cell synapse. Middle: normalized I-V relationship for EPSCs evoked at each of the labeled sites. The dashed red line is the linear regression fit to the current amplitude at negative potentials (−60 to 0 mV). If EPSC amplitudes at positive potentials fall below the red line, these synaptic currents have an inwardly rectifying I-V relationship. Bottom: an example shows the average current traces recorded in the soma (white circle) and evoked at several stimulation sites (colored circles) as labeled in the reconstructed image (top right). Current amplitudes were normalized to the amplitude at −60 mV. At the distal sites the outward currents recorded at +40 mV relative to −60 mV increased.

(B) Left: the rectification index (RI) increases at distal synapses, indicating a greater presence of GluA2-containing AMPARs. Open circles represent the individual measurements (51 sites from 17 stellate cells and 16 mice) and the line shows the segmented average. Right: average RI at the intermediate (40–60 μm) and distal synapses (>60 μm) is significantly larger than the RI at the proximal synapses (14–40 μm) (ANOVA, $p < 0.00001$).

(C) Left: the cumulative distribution of decay time constants for individual evoked EPSCs shows a significant increase in decay time at the intermediate (n = 481 events) and distal synapses (n = 373) compared to proximal sites (n = 862) (#, $p < 0.00005$). Right: the decay time constant increases at distal synapses consistent with the presence of more GluA2-containing receptors (51 sites from 17 cells and 16 mice; ANOVA, $p < 0.005$). Bottom: the evoked EPSC amplitude at −60 mV is shown ($p < 0.05$). Tukey post hoc test:*$p < 0.05$ and ***$p < 0.001$.

(D) Bath application of IEM 1460 (100 μM), a GluA2-lacking AMPAR blocker, produced a greater inhibition at proximal synapses (five sites, one site/cell from five mice) than distal sites (six sites, one site/cell from six mice; $p = 0.005$). Evoked synaptic currents were recorded before (black trace) and during the application of IEM 1460 (at 7.5–15 min, red trace) in the same stellate cells at each dendritic site. A time course of EPSC amplitude plot is shown in Figure S2A.

(E) Non-stationary fluctuation analysis (NSFA) of evoked EPSCs recorded at two dendritic locations. Left: example current traces of NSFA of evoked EPSCs recorded at two dendritic locations (top, 35 μm; bottom, 45 μm) are shown. EPSCs (black lines) are superimposed to scaled average trace of 50 EPSCs (red lines). The difference between each EPSC and the scaled mean is shown as blue lines below. Middle and right: variance in the decay phase of the individual EPSCs around the mean is plotted against the averaged EPSC amplitude to produce the variance – mean current relationship. Red line is the parabolic fit from which mean single-channel current was estimated (closed circles: fitted points of the dataset). 50 (left) and 36 (middle) EPSCs were used for analysis. Right: the mean single-channel conductance of EPSCs decreases at distal synapses (open circles present individual data; ANOVA, $p < 0.0005$, **$p < 0.002$, and ***$p < 0.0005$). See also Figures S1 and S2.

Error bars indicate SEM.

at various potentials. Spermine and other polyamines are known to block AMPARs that do not contain GluA2 at depolarized (>0 mV) potentials, giving rise to a characteristic inwardly rectifying current-voltage (I-V) relationship (Bowie and Mayer, 1995; Kamboj et al., 1995). Synaptic currents evoked by activating parallel fiber axons with a stimulating electrode placed within 40 μm of the soma showed a reduced amplitude at +40 mV, and they exhibited an inwardly rectifying I-V relationship (Figures 1A and 1B; Figure S1A). This suggests that synaptic currents at proximal dendrites are mediated by GluA2-lacking AMPARs. As the stimulating electrode was moved away from the soma of the stellate cell, the EPSC amplitude at positive potentials increased relative to negative potentials and the I-V relationship became more linear. The rectification index (RI) of synapses at distal dendrites (>40 μm; 0.64 ± 0.03; n = 25) was significantly greater than that at proximal dendrites (<40 μm; 0.45 ± 0.02; n = 26; $p < 0.000002$; Figure 1B). Because the change occurred at about 40 μm from the soma, the dendritic region between 40 and 60 μm was considered the intermediate dendritic zone. The change in rectification properties was due to spermine block, because, when a spermine-free pipette solution was used, the I-V relationship of EPSCs was linear and independent of the synaptic distance (Figure S1B). The decay time constant of synaptic currents increased with distance (Figure 1C), consistent with greater GluA2 presence at distal sites. These results indicate that the increase in RI of synaptic currents along dendrites reflects an increase in GluA2 expression.

Second, we used IEM 1460, a GluA2-lacking receptor selective inhibitor to determine subunit composition of synaptic AMPARs. Because EPSCs became more linear at ~40 μm, we compared IEM 1460 inhibitory potency at proximal (<40 μm) and distal (>40 μm) synapses. At proximal dendrites, the amplitude of evoked EPSCs recorded at −60 mV was markedly reduced during the application of 100 μM IEM 1460 (68% ± 3% reduction, n = 5) without an alteration in the failure rate, indicating the prevalence of GluA2-lacking receptors (Figure 1D; Figure S2A) closer to the soma. In contrast IEM 1460 blocked only 46% ± 4% of the synaptic current at intermediate/distal dendritic sites (n = 6; $p < 0.002$). Thus, synaptic AMPARs change from largely GluA2 lacking at proximal synapses to GluA2 containing at more distal synapses.

Third, AMPARs that contain GluA2 subunits have a lower single-channel conductance than GluA2-lacking receptors (Bats et al., 2012). We therefore estimated the mean single-channel conductance (γ) of synaptic AMPARs using peak-scaled, nonstationary fluctuation analysis (NSFA; Benke et al., 1998; Traynelis et al., 1993). We first tested the NSFA method on computer-generated AMPA EPSCs. When simulated AMPA EPSCs were analyzed, both the conductance (5–20 pS) and the number of activated channels (100–200 channels) of the simulated EPSCs were accurately detected using NSFA (Figure S2B). We next performed NSFA on evoked EPSC recordings from slices (Figure 1E) that displayed rapid rise and decay kinetics and that were stable throughout the recording period (mean: 32.5 ± 1.7 events; 36 synapses; Figure S2C). The average γ of EPSCs recorded at proximal dendrites was 14.5 ± 1.0 pS (n = 18). NSFA was then performed to estimate the synaptic conductance at intermediate and distal dendritic sites (>40 μm). The γ of EPSCs decreased at 40–60 μm (8.7 ± 0.7 pS; n = 11; $p < 0.0005$) and at >60 μm (8.6 ± 1.2 pS; n = 7; $p < 0.002$; Figure 1E). There was no correlation between the mean conductance and average EPSC amplitude (Figures S2E and S2F), suggesting variability in the total number of AMPARs between synapses. The smaller conductance at distal synapses was not due to dendritic filtering because prolonging AP duration promoted the expression of inwardly rectifying AMPARs at 40–60 μm and increased the γ of EPSCs (see below). Thus, the difference in conductance is mainly due to a variation in AMPAR composition at synapses. Furthermore the single-channel conductance of EPSCs is greater at synapses with a strong inward rectification and rapid decay time (Figures S2G and S2H), indicating that the distance-dependent increase in EPSC RI is not due to an increase in transmembrane AMPAR regulatory protein (TARP)-AMPAR interactions, which enhance single-channel conductance (Bats et al., 2012). Together our results show that GluA2 expression increases with dendritic distance in stellate cells.

Ca^{2+} Entry during APs Determines the Synaptic AMPAR Phenotype along Dendrites

What physiological stimulus drives the dendritic GluA2 gradient? Cerebellar stellate cells fire APs in the absence of synaptic input (Häusser and Clark, 1997). APs passively spread within the dendrites of stellate cells, and spike amplitude decreases at ~50 μm from the soma in P30–33 rat stellate cells with more complex dendritic structures and longer dendrites than post-natal day (P)17–19 rat stellate cells (Myoga et al., 2009). We characterized the morphology of stellate cell dendrites from P18–23 mice. Stellate cells filled with Alexa 594 had 3.5 ± 0.4 primary dendrites with an average length of 81.2 ± 6.2 μm (n = 29 dendrites, eight cells; Figure S3A). Dendrites were branched with 2.4 ± 0.5 secondary branches (secondary dendrites) per primary dendrite. Similar morphological features also were found in stellate cells in 18 days in vitro (DIV) cultures (Figure S3B). This dendritic branching pattern matches that of stellate cells from P30–33 rats (3.8 primary dendrites with an average length of 90 μm and 2.4 secondary branches per primary dendrite; Myoga et al., 2009).

Thus, P18–23 mouse stellate cells have a dendritic branching pattern similar to mature rat stellate cells, and in the latter the AP amplitude decreases in the dendrites (Myoga et al., 2009). To determine whether somatic APs also fail to elicit a Ca^{2+} rise at distal dendrites in mouse stellate cells, we evoked five somatic APs at 100 Hz and measured the amplitude of the Ca^{2+} transients (expressed as ΔF/F) along the dendrites. For these experiments, stellate cells were filled with Oregon Green BAPTA-1 (100 μM), and Ca^{2+} transients were detected using a multi-photon line scan at various dendritic locations (Figures 2A and 2B). We observed the largest Ca^{2+} peaks at the most proximal sites (with an average ΔF/F of 35% ± 2% for distances ≤20 μm; n = 14); the amplitude of dendritic Ca^{2+} transients progressively decreased with the distance from the soma, with the steepest decrease after 40 μm (Figure 2C). The Ca^{2+} signal became undetectable from baseline for distances ≥70 μm. This marked attenuation of the amplitude of the Ca^{2+} transients along the dendrites suggests that somatic APs failed to back-propagate or were unable to activate a significant number of voltage-dependent Ca^{2+} channels in the distal dendrites.

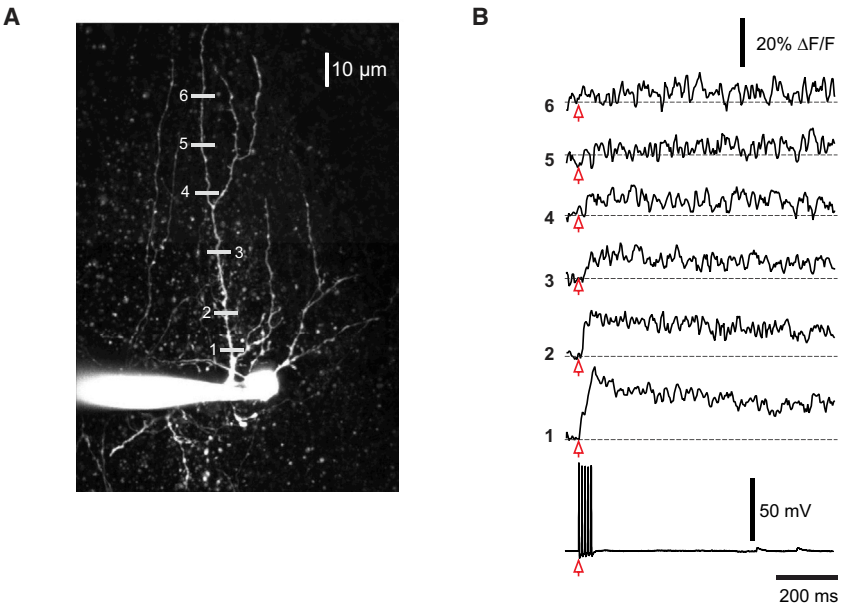

Figure 2. The Amplitude of Ca^{2+} Transients Generated in Response to Somatic APs Decreases with the Distance along the Dendrites of Stellate Cells

(A) Two-dimensional projection of a two-photon 3D z stack for a stellate cell filled with Oregon Green BAPTA-1 (100 µM). The gray lines represent the dendritic regions where the Ca^{2+} transients were measured using line scans.

(B) Ca^{2+} transients (expressed as ΔF/F) generated in response to a 100-Hz train of five somatic APs (lower voltage trace). The numbers on the left of the traces refer to the locations of the line scans in (A).

(C) Plot of the mean amplitude of the peak of the Ca^{2+} transients associated with the train of five back-propagating APs as a function of the distance from the soma. The values of ΔF/F were binned into 10-µm intervals (20 µm for the most distal locations, ≥70 µm) and averaged. Open circles represent the individual measurements (63 sites from 11 stellate cells and eight mice).

(D) The decrease in dendritic Ca^{2+} transients is spatially correlated with an increase in the RI of EPSCs.

Error bars indicate SEM.

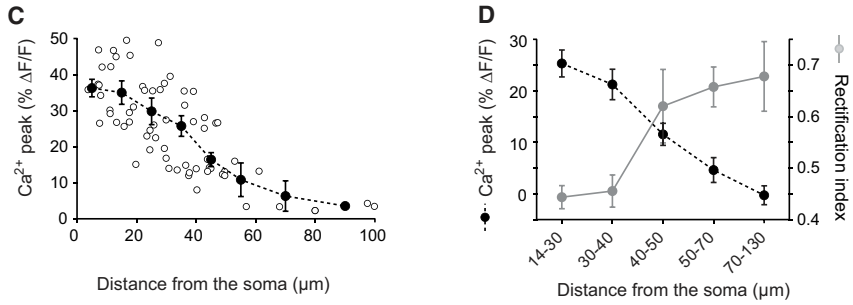

The decrease in dendritic Ca^{2+} transients generated in response to somatic APs was spatially correlated with an increase in the RI of EPSCs along dendrites (Figure 2D). We therefore tested the possibility that attenuation of APs in mouse stellate cells leads to an increase in GluA2 expression at distal dendrites. We reasoned that increasing the spike duration would allow the depolarization to propagate further along the dendrites and thereby shift the dendritic GluA2 gradient toward more distal regions. Our recent study shows that application of the potassium channel blocker tetraethylammonium (TEA) increases the AP width in stellate cells and enhances Ca^{2+} entry via voltage-gated Ca^{2+} channels by 40% without changing the frequency of spontaneous APs, inhibitory postsynaptic currents (IPSCs), and EPSCs (Liu et al., 2011). We therefore incubated cerebellar slices with TEA (1 mM). Since increasing AP duration also promotes GluA2 gene expression in stellate cells (Liu et al., 2010), actinomycin D, a transcriptional inhibitor, was included during TEA incubation to inhibit gene transcription. Furthermore, to minimize any presynaptic effects of TEA, we included picrotoxin (PTX) and kynurenic acid (KYNA) to block $GABA_A$ and ionotropic glutamate receptors, respectively, in both control conditions and during TEA incubation.

Incubation of cerebellar slices with actinomycin D (25 µM + PTX + KYNA) alone for 3 hr did not alter the I-V relationship of EPSCs or the distance-dependent increase in the RI (Figure 3C; Figures S4A and S4B). However, following a 3-hr incubation with 1 mM TEA (+ actD + PTX + KYNA), we found that synapses located at 40–60 µm from the soma became more inwardly rectifying than controls (Figure 3A), consistent with a decrease in GluA2 levels. The decay time constant of EPSCs was more rapid after TEA treatment relative to actinomycin D (+ PTX + KYNA) control at 40–60 µm, also consistent with a local GluA2 decrease, whereas no difference was observed at synapses in proximal dendrites (<40 µm; Figure 3B). A stronger inward rectification and more rapid decay time of EPSCs suggest an increase in GluA2-lacking receptors at 40–60 µm following TEA treatment. This hypothesis would predict a greater single-channel conductance of EPSCs at intermediate dendritic sites. To test this idea, we determined mean single-channel conductance of EPSCs using NSFA. TEA treatment disrupted the gradient of channel conductance seen in control cells (Figure 3D), and single-channel conductance at 40–60 µm increased to 12.5 ± 1.0 pS (n = 5) from control 8.7 ± 0.7 pS (n = 11; $p < 0.01$). Thus, prolonging the duration of APs can extend the expression of GluA2-lacking AMPARs to a more distal dendritic site than in control cells.

We next examined whether Ca^{2+} entry during APs drives the expression of GluA2-lacking AMPARs at the proximal dendrites. Ca^{2+} enters the dendrites of stellate cells via voltage-gated Ca^{2+} channels during APs (Figure 2; Myoga et al., 2009). N-type Ca^{2+} channels are expressed in stellate cells (Tharani et al., 1996).

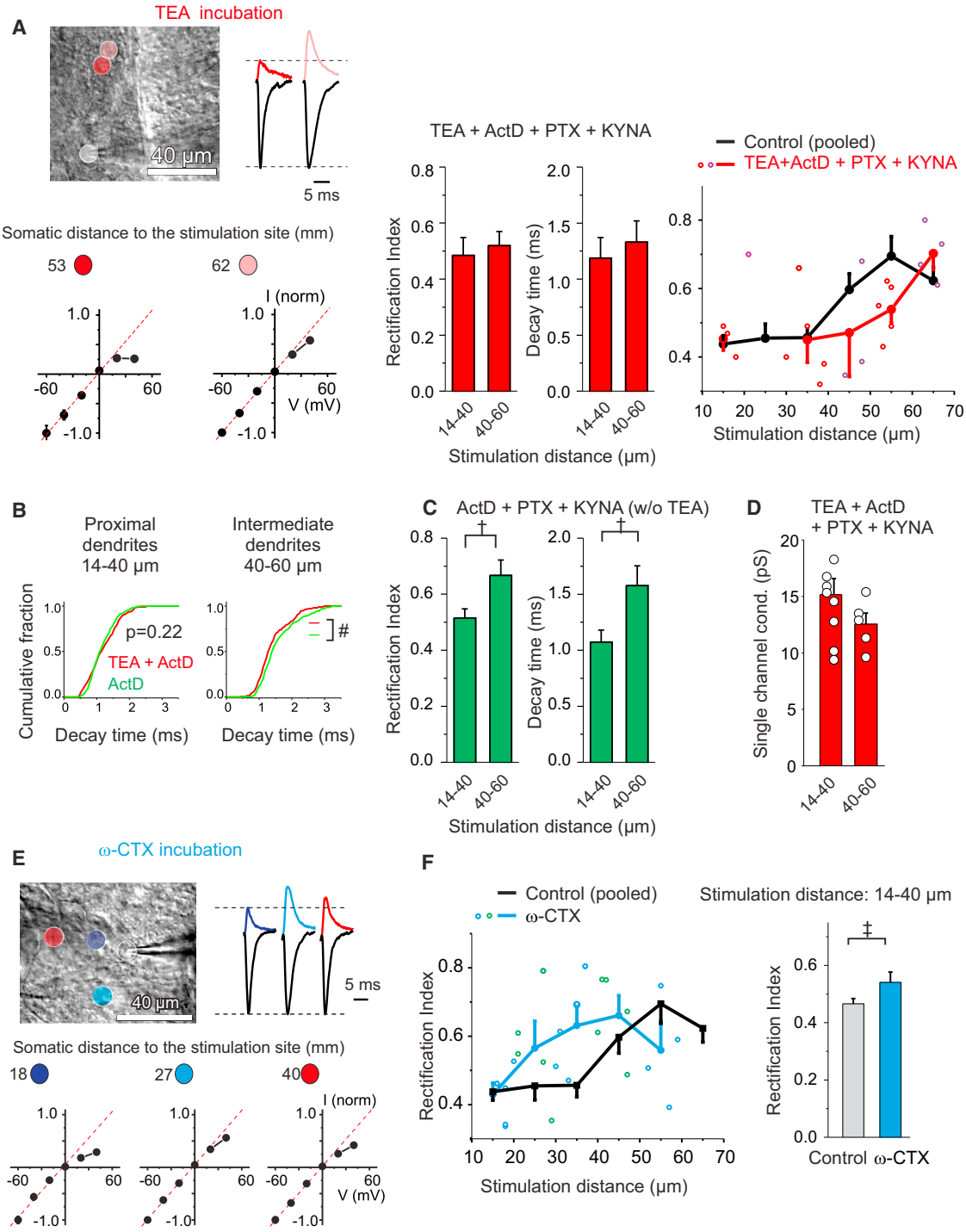

Figure 3. Ca^{2+} Entry during APs Determines Synaptic AMPAR Phenotype along Dendrites

(A) Cerebellar slices were incubated with 1 mM tetraethylammonium (TEA) in the presence of 25 µM actinomycin D (actD), 100 µM picrotoxin (PTX), and 1 mM kynurenic acid (KYNA) for 3 hr to increase the duration of APs and enhance Ca^{2+} entry (Liu et al., 2010). Left: example of recordings at two locations and corresponding I-V relationship show a decrease in outward current (at +40 mV) relative to current at −60 mV at the intermediate stimulation distance. Middle: the average RI and decay time constant of EPSCs did not increase at 40–60 µm (23 sites from eight cells and eight mice). Right: increasing AP duration by TEA treatment shifted the dendritic GluA2 gradient toward more distal regions. Data from actD (+ PTX + KYNA) treated and control in Figure 1B were not different from each other (Figures S4A and S4B) and were shown as a combined control. Adjacent bins' data points are labeled red/purple.

(legend continued on next page)

Following incubation of slices with 500 nM ω-conotoxin GVIA, an N-type Ca^{2+} channel blocker, for 3 hr, the I-V relationship of EPSCs became more linear in the proximal dendrites relative to control (Figures 3E and 3F). Thus, blocking N-type Ca^{2+} channels elevated synaptic GluA2 receptors in proximal dendrites and disrupted the gradient of synaptic GluA2 levels along the dendrites. These results indicate that Ca^{2+} entry during APs suppresses GluA2 expression or promotes GluA2-lacking receptors in proximal dendrites. Thus, in contrast to a previously described presynaptic mechanism in which elevated presynaptic activity increases synaptic GluA2 expression (Liu and Cull-Candy, 2000), postsynaptic APs suppress synaptic GluA2 levels, producing an opposite synaptic phenotype.

Synaptic activity also can increase the expression of GluA2-containing receptors at stellate cell synapses (Liu and Cull-Candy, 2000). We found that incubation with glutamate receptor and $GABA_A$ receptor blockers KYNA and PTX, in the presence of actinomycin D, for 3 hr did not alter the pattern of synaptic GluA2 expression (Figure 3C; Figure S4A). We did not observe any difference in the paired-pulse ratio and the failure rate of EPSCs evoked at proximal and distal dendrites (Figure S4C), suggesting no apparent difference in glutamate release between the proximal and distal synapses. Thus, synaptic activity is unlikely to drive the observed GluA2 gradient along the dendrites.

Spontaneous AP Firing Drives Synaptic AMPAR Subtype Gradient via CPEB3

Thus far we found that synaptic AMPAR subtypes are differentially distributed along dendrites, with GluA2-lacking receptors at proximal dendrites and GluA2-containing receptors at distal dendrites. We also observed that inhibition of gene transcription with actinomycin D (+ PTX + KYNA) did not disrupt the GluA2 gradient along dendrites (Figure 3C; Figure S4A). We therefore tested the effects of a protein synthesis inhibitor, cycloheximide, on the dendritic distribution of GluA2 receptors when spermine was included in the pipette solution. Following incubation of cerebellar slices with cycloheximide for 3 hr, we observed no gradient in the RI of EPSCs along dendrites. Synaptic currents at a dendritic distance >40 μm became more inwardly rectifying than controls, with no alteration in the synaptic current amplitude (Figures 4A and 4B; Figure S4D). Protein synthesis is thus required for the expression of GluA2 receptors in distal dendrites and for the establishment of the GluA2 gradient along dendrites.

Protein synthesis of GluA2 subunits is regulated by an RNA-binding protein, CPEB3 (Huang et al., 2006; Theis et al., 2003). We therefore tested whether CPEB3-GluA2 mRNA interactions could be responsible for the dendritic GluA2 gradient by suppressing synaptic GluA2 expression at proximal dendrites. First, does disruption of CPEB3-GluA2 mRNA interaction increase synaptic GluA2 content at proximal dendrites? Second, does AP firing regulate CPEB3 expression and thereby change AMPAR subtype?

Disruption of CPEB3-GluA2 mRNA Interaction Increases Synaptic GluA2 Expression at Proximal Synapses

To acutely disrupt a CPEB3-GluA2 mRNA interaction, we used a 49-nt oligomer, SELEX 1904, which previously was shown (Huang et al., 2006) to selectively compete with GluA2 mRNA for binding to CPEB3. We included a low concentration of SELEX 1904 in the patch electrode solution (10 μM) to disrupt the CPEB3-GluA2 mRNA interaction, and we monitored changes in the I-V relationship of EPSCs at proximal dendrites (<40 μm; Figure 4C) over time. The I-V relationship of EPSCs was inwardly rectifying during the first 30 min and became more linear by 60–90 min (Figures 4D and 4E). Synapses that showed stronger inward rectification at the beginning of recording also had a greater increase in the RI (Figure 4F). As a control for any nonspecific effects, the inclusion of an oligomer that does not bind to CPEB3 in the pipette solution (10 μM) did not alter the RI of EPSCs over the time course of the recording (Figures 4D–4F).

If SELEX 1904 disrupts the CPEB3-GluA2 mRNA interaction and thereby increases GluA2 synthesis, the SELEX 1904-induced change should be prevented by protein synthesis inhibitors. Indeed, when anisomycin was applied prior to and throughout the duration of the recording, intracellular SELEX 1904 application failed to alter the RI of EPSCs (Figure 4D; Figure S4E). Therefore, the CPEB3-GluA2 mRNA interaction in stellate cells prevents the synaptic expression of GluA2 by suppressing GluA2 protein synthesis. Increasing GluA2 expression by selective disruption of this interaction (and without interfering with any of the known mechanisms for GluA2-containing AMPAR insertion) indicates that regulation of GluA2 translation is required.

Blocking Postsynaptic Activity with Tetrodotoxin Increases Synaptic GluA2 AMPARs and Reduces CPEB3 Expression

Our results suggest that an AP-driven Ca^{2+} influx reduces the proximal synaptic GluA2 content (Figure 3) and this requires CPEB3-mRNA binding (Figure 4). Failure of spontaneous AP propagation to distal dendrites elevated synaptic GluA2 expression (Figure 3). We hypothesized that postsynaptic spiking activity in stellate cells shifts AMPAR-GluA2 composition by promoting local CPEB3 expression. To determine the effect of APs on CPEB3 expression, we therefore tested whether the inhibition of somatic AP firing would increase synaptic GluA2 content and reduce the CPEB3 level in the soma of stellate cells.

(B) The decay time constants for individual EPSCs were significantly reduced at the intermediate dendrites (40–60 μm) following TEA + ActD treatment relative to ActD control (#$p < 0.01$, 203 and 248 events, respectively), consistent with a decrease in synaptic GluA2.
(C) The RI and decay time constant of EPSCs increased at intermediate synapses in ActD-treated control (20 sites from eight cells and eight animals).
(D) Following TEA treatment, the mean single-channel conductance of EPSCs at 40–60 μm was no longer reduced compared to proximal synapses.
(E and F) Cerebellar slices were treated with an N-type Ca^{2+} channel blocker, ω-conotoxin GVI-A (ω-CTX, 500 nM) for 3 hr. I-V relationship for EPSCs evoked at the proximal sites became more linear following ω-CTX treatment (17 proximal sites and 12 distal sites from 12 cells and nine mice). Open circles represent the individual measurements; adjacent bins' data points are labeled blue/green ($p < 0.05$). See also Figure S4.
Error bars indicate SEM.

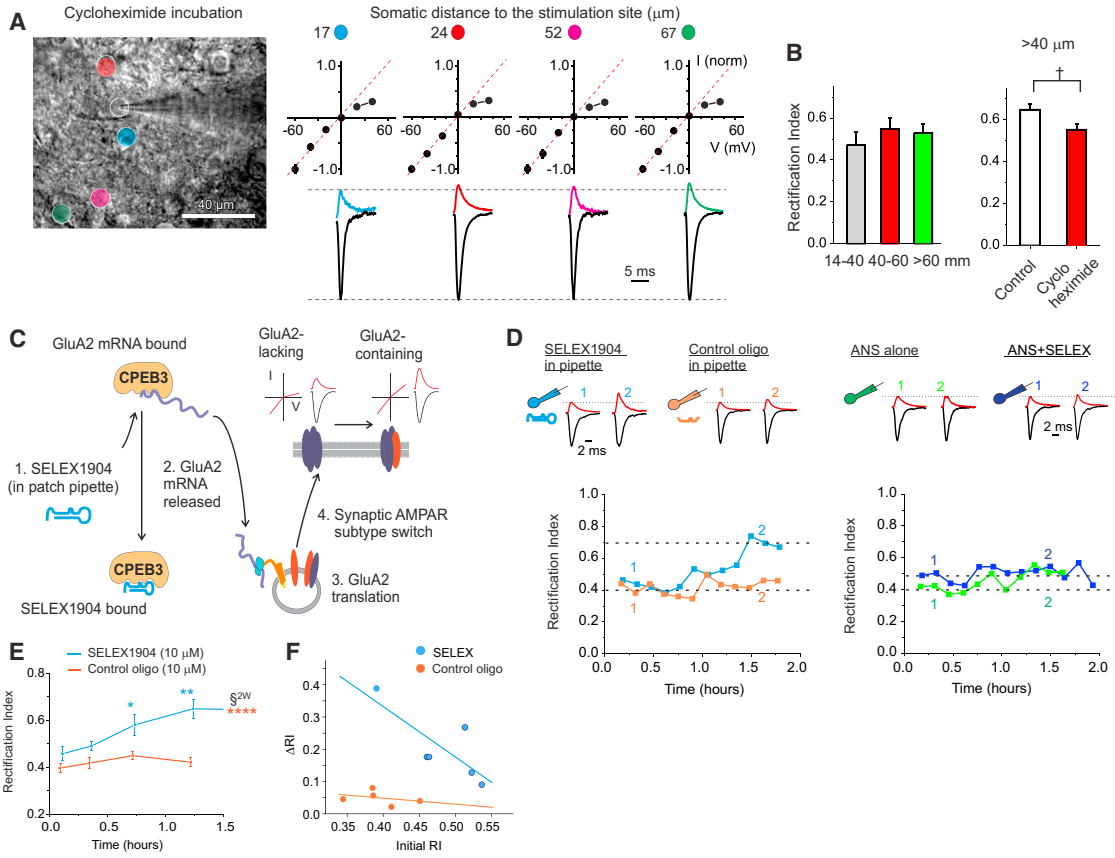

Figure 4. Disruption of the CPEB3-GluA2 mRNA Interaction Enhances Synaptic GluA2 Expression at the Proximal Dendrites in a Protein Synthesis-Dependent Manner

(A) Cerebellar slices were incubated with 100 μM cycloheximide (CHX) for 3 hr and then synaptic currents were recorded and evoked at the stimulation sites labeled in the left panel. Spermine (100 μM) was included in the pipette solution to block synaptic GluA2-lacking receptors at positive potentials. Right: average EPSC traces recorded at +40 and −60mV and corresponding I-V relationship are shown.

(B) The increase in the RI of EPSCs at the distal synapses was abolished following CHX treatment (seven sites for proximal; six for intermediate; four sites for distal from six cells; six mice), and EPSC RI at >40 μm was reduced compared to control ($p < 0.05$).

(C) SELEX 1904 is an RNA oligomer that competes with GluA2 mRNA for binding to CPEB3 (Huang et al., 2006). If CPEB3 binding with GluA2 mRNA prevents GluA2 protein synthesis at proximal synapses, SELEX 1904 should increase synaptic GluA2 expression in stellate cells.

(D) Left: example of evoked EPSCs at a proximal synapse. Including SELEX 1904 (10 μM) in the pipette solution increased EPSC amplitude at +40 mV, and the I-V relationship of EPSCs became more linear with time, indicating an increase in synaptic GluA2 receptors. Control oligo sequence was identical to SELEX 1904, but it was missing several terminal nucleotides needed to stabilize the hairpin 3D conformation that disrupts CPEB3/GluA2 mRNA interaction (see the Experimental Procedures). Right: anisomycin (ANS), when added to ACSF prior to and during recording, prevented the SELEX-induced increase in EPSC RI.

(E) RI of EPSCs remained unaltered during the first 30 min and then gradually increased at proximal dendrites (<40 μm; n = 6). A control oligomer (10 μM) did not alter the amplitude (B) and RI of EPSCs (n = 5; two-way ANOVA, $p < 0.0005$ for treatment groups and for time bins; Tukey means comparison versus either control, *$p < 0.01$, **$p < 0.005$, or versus time bin 1, ***$p < 0.0005$).

(F) The initial RIs are those recorded within 15 min (four cells) and between 15–30 min (two cells in which we were unable to find the inputs within 15 min) after obtaining the whole-cell configuration. Change in RI (ΔRI) was calculated as a difference between the average RI after it reached a plateau and the initial RI (linear regression for SELEX, $R^2 = 0.62$ and for CTL oligo, $R^2 = 0.11$). See also Figure S4.

Error bars indicate SEM.

We directly examined whether somatic APs controlled the synaptic AMPAR phenotype by using tetrodotoxin (TTX). TTX inhibits spiking activity not only in postsynaptic stellate cells but also silences presynaptic neurons. This causes a reduction of neurotransmitter release, which may influence postsynaptic AMPAR phenotype in stellate cells (Liu and Cull-Candy, 2000). We therefore added $GABA_A$ and ionotropic glutamate receptor blockers PTX and KYNA in both control conditions and during TTX incubation for 3 hr. TTX and KYNA were washed out prior to recordings. While evoked EPSCs were used as a direct readout of synaptic properties at known distances along the dendrites in the results shown so far (Figures 1, 2, 3, and 4), spontaneous EPSCs (sEPSCs; Figure 5) provided a measure of the intrinsic activity of all synapses onto stellate cells. The sEPSCs enable a comparison of the average EPSCs (average synapse on the cell) recorded under different experimental conditions, and they were

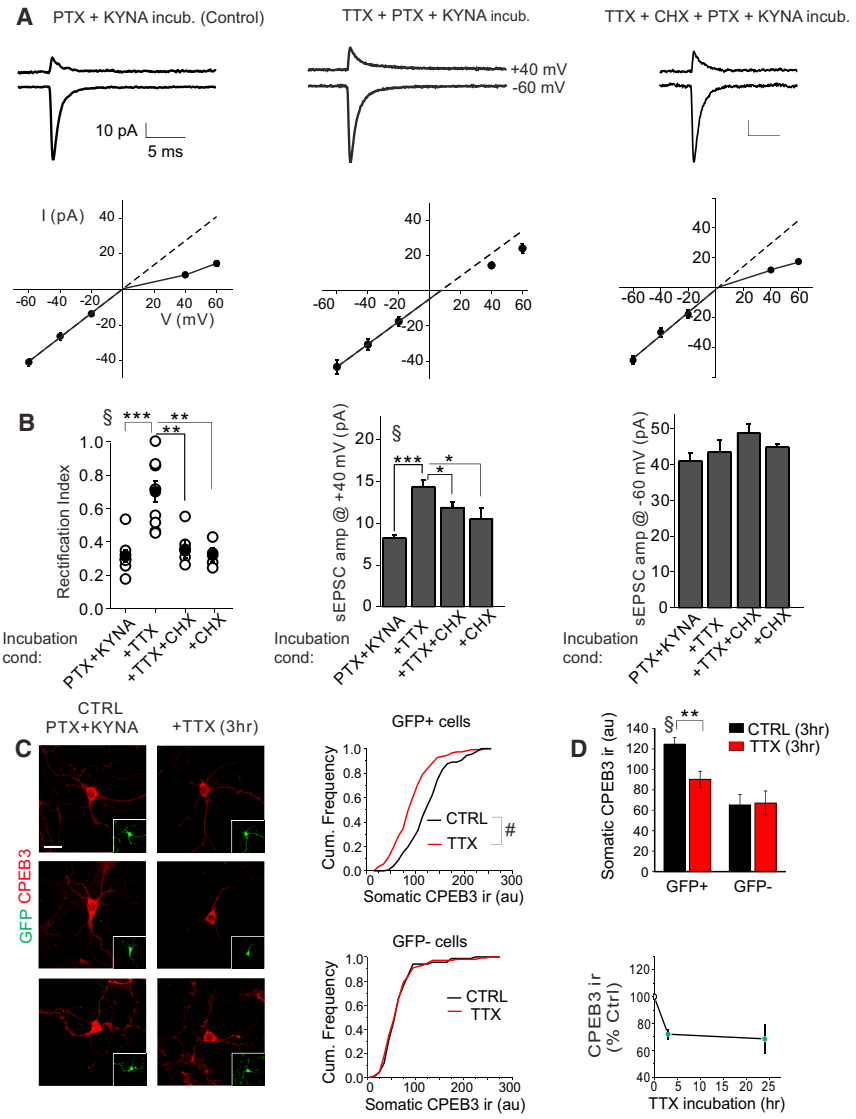

Figure 5. TTX Treatment Enhances the Protein Synthesis-Dependent Expression of GluA2-Containing AMPARs at Synapses and Reduces the Level of CPEB3 Expression in Stellate Cells

(A) Slices were pretreated with 1 mM KYNA and 100 μM PTX without (control) or with 0.5 μM tetrodotoxin (TTX) for 3 hr. Right: slices were treated with TTX in the presence of a protein synthesis inhibitor (100 μM CHX) for 3 hr. Average current traces recorded at +40 and −60 mV and the I-V relationship of AMPAR-mediated sEPSCs in stellate cells are shown. TTX treatment increased rectification of EPSCs, which was prevented by CHX.

(B) Summary data. Left: RI of individual cells (open circles) and average value (filled circle) are shown. Middle and right: EPSC amplitudes at +40 and −60 mV (cont, n = 8; TTX, n = 10; TTX + CHX, n = 6; CHX, n = 4;) are shown (ANOVA, $p < 0.0001$; Tukey post hoc, *$p < 0.05$, **$p < 0.005$, and ***$p < 0.0005$).

(C) Cerebellar cultures were prepared from GAD-65 mice, in which stellate cells expressed GFP and GFP-negative neurons were mainly granule cells. TTX treatment for 3 hr reduced CPEB3-ir in GFP-positive cells. Left: CPEB3-ir is shown. Insets show GFP. Right: comparison of somatic CPEB3-ir in TTX-treated versus control stellate cells (GFP+) and granule cells (GFP−, bottom) (GFP+, >120 cells, $p < 0.00001$; GFP−, 67 control and 100 TTX-treated cells from three cultures).

(D) Effects of TTX treatment on CPEB3-ir levels in GFP+ cells and GFP− cells. Bottom: prolonged incubation with TTX for 24 hr did not further reduce the CPEB3 levels in GFP+ cells (three cultures). ANOVA, $p < 0.002$; post hoc test, **$p < 0.005$. Scale bar, 12 μm. See also Figures S5–S7.

Error bars indicate SEM.

therefore used to investigate the molecular mechanisms by which somatic APs control synaptic AMPAR subtype expression.

The sEPSCs in stellate cells displayed an inwardly rectifying I-V relationship, consistent with the presence of GluA2-lacking AMPARs. Incubation with PTX and KYNA did not alter the RI of sEPSCs (0.32 ± 0.04 [n = 8] versus without PTX and KYNA, 0.34 ± 0.05; Liu et al., 2010; Figure 5A) or current amplitude (−40.8 ± 2.2 versus without PTX and KYNA, −47.0 ± 3.2 pA). However, following TTX treatment, the sEPSC amplitude increased at +40 mV (at this potential synaptic currents are mediated mainly by GluA2-containing receptors) from 8.3 ± 0.4 to 14.4 ± 0.9 pA ($p < 0.00005$; control, n = 8; TTX, n = 10), but it remained unaltered at −60 mV (Figure 5B). Consequently, the I-V relationship of sEPSCs became more linear and the RI increased to 0.70 ± 0.06 ($p < 0.0001$; Figure 5B). Furthermore, the decay time of sEPSCs was prolonged after TTX treatment (Figure S6A). These results indicate that TTX treatment increased the synaptic expression of GluA2-containing receptors.

In addition to inclusion of GluA2 subunits, the interaction of TARP with GluA2-lacking receptors can produce a moderate increase in the RI (Soto et al., 2007). Since 6-Cyano-7-nitroquinoxaline-2,3-dione (CNQX) acts as an AMPAR partial agonist in the presence of TARP, a CNQX-evoked inward current is diagnostic for the association of TARP with AMPARs (Menuz et al., 2007). We therefore tested whether the TTX-induced change involved an increased interaction with TARP by examining the CNQX-induced AMPAR-mediated increase of the holding current in stellate cells. Bath application of CNQX and cyclothiazide (to reduce AMPAR desensitization) elicited an additional inward current (44.2 ± 17.3 pA; n = 4), which was not enhanced after the TTX treatment (48.9 ± 11.0 pA; n = 5; Figure S6B) but was blocked by AMPAR antagonist GYKI. Thus, the increase in EPSC RI is unlikely to result from an increase in a TARP-AMPAR association.

This result, together with the two opposing effects on the dendritic GluA2 gradient by TEA and an N-type Ca^{2+} channel blocker (Figure 3), suggests that postsynaptic APs and the associated Ca^{2+} influx are critical for controlling synaptic GluA2 expression and establishing a distance-dependent distribution of synaptic AMPAR subtypes along dendrites.

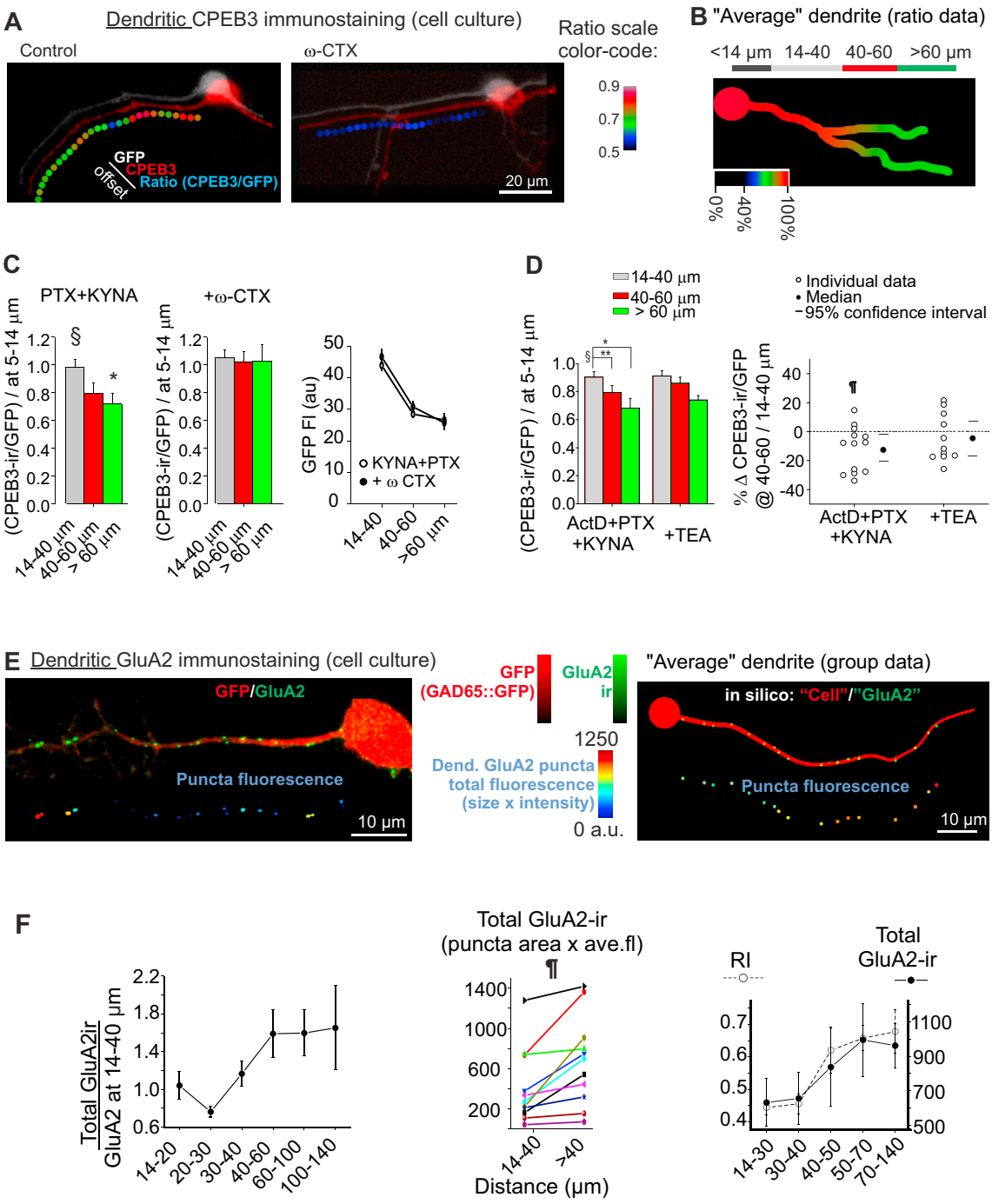

Figure 6. Immunohistochemical Gradients of CPEB3 and GluA2 Proteins in Stellate Cell Dendrites

(A) Examples of dendritic CPEB3-ir in GFP+ neurons in cerebellar cultures. CPEB3/GFP ratio was calculated by dividing the corresponding signals in each region of interest (ROI) (see the Experimental Procedures for details). Individual channels (GFP-ir, CPEB3-ir, color-coded ratio) are diagonally offset for illustration purposes. Left: control CPEB3 staining showed a distance-dependent decrease toward the distal dendritic regions (3-hr incubation in PTX + KYNA). Right: the CPEB3-ir decrease was attenuated by incubating cells in 500 nM ω-conotoxin GVIA (ω-CTX) prior to immunostaining for CPEB3 (3-hr incubation in ω-CTX + PTX + KYNA).

(B) The ratio of CPEB3-ir/GFP fluorescence intensity was used to quantify the CPEB3 expression at various segments along the dendrites and was normalized to the value at 5–14 μm from the soma for each dendritic process. Right: group data are shown, represented as a color gradient of an average schematic dendrite.

(C) CPEB3-ir decreased at more distal dendrites (>60 μm) in control (n = 19 from seven cultures; one-way ANOVA, $p < 0.05$; Tukey post hoc, 14–40 versus >60 μm, $p < 0.05$), which was abolished following ω-CTX treatment (n = 14 from six cultures). *$p < 0.05$ and ***$p < 0.005$. Right: dendritic GFP fluorescence did not change after ω-CTX treatment.

(legend continued on next page)

We have shown that inhibition of protein synthesis reduced the expression of synaptic GluA2 in distal dendrites (Figure 4B), suggesting that an increased expression of GluA2 at distal synapses requires protein synthesis. We hypothesized that attenuation of AP back-propagation may enhance local GluA2 synthesis and thereby synaptic GluA2 expression at distal synapses. This model predicts that suppressing somatic APs would enhance the expression of synaptic GluA2 expression by promoting protein synthesis. Cerebellar slices were incubated with TTX (PTX + KYNA) in the presence of cycloheximide (100 μM), a protein synthesis inhibitor. After this treatment, synaptic currents had an inwardly rectifying I-V relationship (RI, 0.37 ± 0.04; n = 6; versus TTX $p < 0.005$; Figure 5A) in contrast to the usual TTX-induced linear relationship. Cycloheximide prevented the TTX-induced increase in EPSC amplitude at +40 mV (11.3 ± 0.6 pA; $p < 0.05$; Figure 5B). A second protein synthesis inhibitor, anisomycin (40 μM), also prevented the increase in RI (0.33 ± 0.04, n = 5; $p < 0.0005$) that was induced by TTX treatment (Figure S6C). Incubation with anisomycin and cycloheximide alone did not alter the EPSC RI (Figure 5B; Figures S5C and S5D). These results indicate that silencing AP firing increases synaptic GluA2-containing receptors via a protein synthesis-dependent process.

We next determined the effect of spontaneous APs on CPEB3 expression in stellate cells. Cerebellar cultures were prepared from GAD65::GFP knockin mice (expressing intracellular GFP under the GAD67 promoter), in which the GFP-positive cells are stellate cells and GFP-negative neurons are mainly granule cells. Stellate cells in culture also exhibited tonic firing, with a spontaneous AP firing frequency (Figure S6A) indistinguishable from that observed in slices (Liu et al., 2010). Cerebellar cultures were incubated with TTX in the presence of PTX and KYNA to block inhibitory and excitatory transmission for 3 hr. This treatment increased the RI of sEPSCs and elevated the current amplitude at +40 mV (Figure S6B), and, thus, stellate cells in both cultures and slices are regulated by APs. We therefore determined whether TTX treatment regulates CPEB3 expression in cultured stellate cells. Incubation with PTX and KYNA did not alter the CPEB3 immunoreactivity (ir) in stellate cells (Figure S7B). Following TTX treatment, the level of CPEB3-ir in the soma of GFP-positive neurons decreased by 27.9% ± 3.3% relative to controls that were incubated in PTX and KYNA ($p < 0.01$; Figure 5C). In contrast GFP signals remained unaltered (Figure S7F). The CPEB3 expression in stellate cells decreased rapidly within 3 hr of TTX application, but prolonged incubation with TTX for 24 hr did not further reduce CPEB3 levels (Figure 5D). Therefore, blocking AP firing reduced overall expression of CPEB3 in stellate cells. Because Ca^{2+} is known to activate elongation factor 2 (eEF2) kinase, a Ca^{2+}/calmodulin-dependent protein kinase that phosphorylates eEF2 and thereby suppresses protein synthesis (Sutton et al., 2007), we examined the level of phosphorylated eEF2, the inactive form of eEF2. We found that TTX treatment did not alter the levels of somatic peEF2-ir in stellate cells (Figure S7C), while incubation with NH125, an eEF2 kinase inhibitor, as a positive control reduced peEF2 levels.

In contrast to stellate cells, cerebellar granule cells do not fire APs without synaptic input and express GluA2-containing receptors. If spontaneous AP spiking activity in stellate cells is indeed responsible for an elevated CPEB3 expression, blocking AP firing should not alter CPEB3 expression in granule cells. As predicted, CPEB3-ir in GFP-negative cells was indeed unaltered by TTX incubation (Figures 5C and 5D; Figure S7D). Together these results support the idea that postsynaptic activity drives the expression of CPEB3. Our results are consistent with a model in which somatic APs elevate CPEB3 at proximal dendrites and attenuation of retrograde APs lowers the CPEB3 expression at distal dendrites, thereby controlling the GluA2 gradient.

We therefore tested a prediction of this model, which is that the CPEB3 level at proximal dendrites should be higher than at distal sites and should be reduced by the inhibition of Ca^{2+} channel activity. We first determined whether the level of CPEB3 expression was lower in distal dendrites than in proximal dendrites. Cultured stellate cells from GAD67::GFP mice were immunostained for CPEB3, and the local dendritic intensity of CPEB3-ir was normalized to that of the GFP signal (i.e., the CPEB3-ir/GFP ratio). We found that the normalized CPEB3-ir was high in proximal dendrites and decreased by 20% ± 7% at 40–60 μm and 28% ± 8% at >60 μm (Figures 6A–6C; repeated-measures [RM] ANOVA, $p < 0.005$; n = 19 dendrites). The magnitude of the reduction in CPEB3-ir at distal dendrites (where AP propagation is attenuated) fits well with our prediction since the somatic CPEB3-ir also was reduced by 20%–30% when APs were blocked with TTX (Figures 5C and 7D). This CPEB3-ir gradient along stellate cell processes was abolished by the inhibition of N-type Ca^{2+} channels with ω-conotoxin GVIA for 3 hr (Figure 6C, middle), while the GFP levels in

(D) Effects of TEA treatment on the CPEB3-ir along dendrites. Cultures were treated with ActD, (+ KYNA and PTX) as control or with the addition of 1 mM TEA for 3 hr. Left: CPEB3-ir decreases at intermediate (40–60 μm) and distal (>60 μm) dendrites relative to proximal dendrites (14–40 μm) in control (n = 13; RM ANOVA, $p < 0.002$; Tukey post hoc test, $^{*}p < 0.05$ and $^{**}p < 0.005$). However, following TEA treatment, CPEB3-ir did not decrease at intermediate sites (n = 11; RM ANOVA, $p = 0.055$). Right: changes in CPEB3-ir at 40–60 μm relative to 14–40 μm of individual dendritic processes are shown. One sample Wilcoxon signed-rank test, $^{\dagger}p < 0.05$.

(E) Left: distal dendrites of stellate cells show an increase in GluA2-ir staining. Top: a representative example of surface GluA2 staining in GAD65::eGFP stellate cell is shown. Bottom: the dendritic GluA2 puncta were color coded for total GluA2-ir fluorescence (area × average intensity), corresponding to the total number of GluA2 molecules present at the synapse. Right: artificially constructed image shows the predicted distribution of GluA2 puncta along an average dendrite, modeled on an increase in 30% puncta size and 20% intensity (Figure S8C). This example illustrates that it is difficult to visually observe the resulting 60% GluA2 increase at distal synapses by eye, yet it is amenable to computer-assisted detection (see the Experimental Procedures for explanations).

(F) Left: total GluA2-ir fluorescence along a dendritic process increased with the distance from the soma (11 processes from five cultures). Middle: total GluA2-ir of individual processes for proximal versus distal puncta is shown (paired Wilcoxon signed-rank test, $p < 0.005$). Right: both RI in slices (see Figure 1) and GluA2-ir showed a similar increase with the dendritic distance. See also Figure S8.

Error bars indicate SEM.

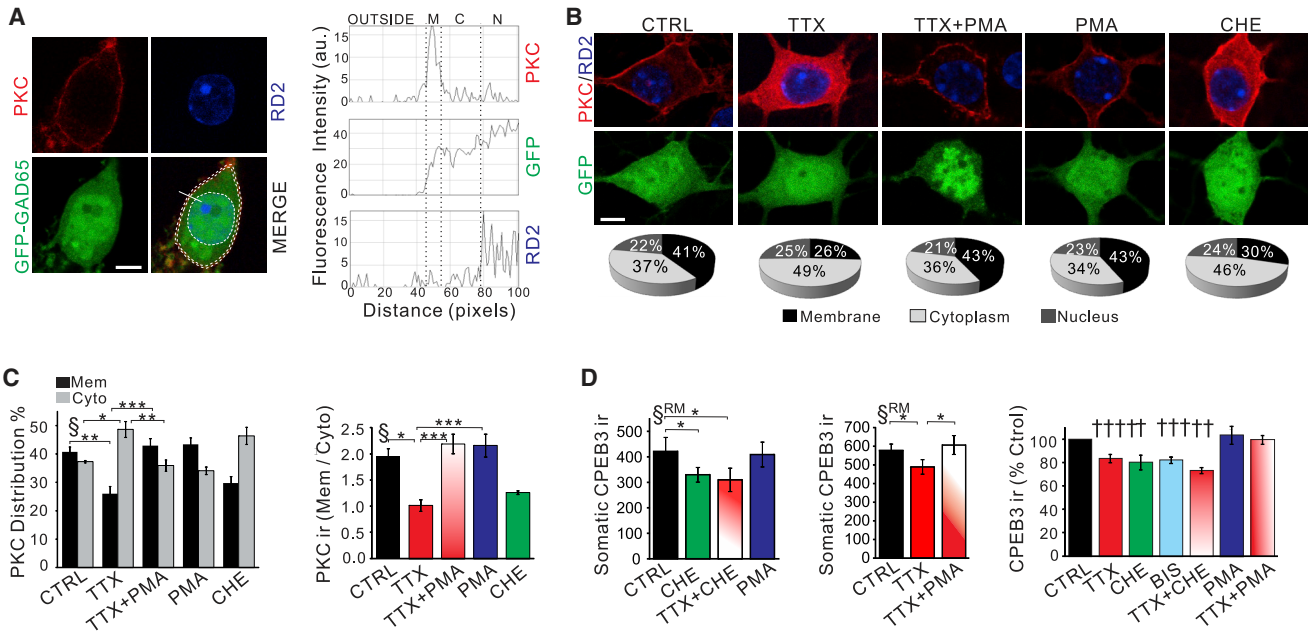

Figure 7. Spontaneous APs Regulate the Expression of CPEB3 via the Activation of PKC

(A) Quantification of PKC-ir. Left: confocal images show a GABAergic interneuron (GFP). Dashed lines outline each compartment. Right: line scans show the levels of PKC-ir, GFP, and RedDot2 (RD2 for nuclear staining) across the soma.

(B) Translocation of PKC to the cytoplasm after TTX treatment. Top: PKC-ir in GFP neurons treated with TTX or PKC modulators is shown. Bottom: distribution of PKC-ir in each compartment is shown.

(C) Left: mean membrane and cytoplasmic PKC-ir levels. Right: the PKC_{memb}/PKC_{cyto} ratio is shown. TTX treatment reduced membrane staining and increased cytoplasmic CPEB3-ir, thereby lowering the PKC_{memb}/PKC_{cyto} ratio. These changes were reversed by co-application of PMA and TTX. Chelerythrine (CHE) or bisindolylmaleimide (BIS), PKC inhibitors, also reduced cytoplasmic translocation of PKC and the PKC_{memb}/PKC_{cyto} ratio.

(D) Effect of the same treatments on CPEB3-ir level is shown (more than three cultures). Scale bars, 5 μm (A and B). C (ANOVA, $p < 0.002$), D (RM ANOVA, $p < 0.02$); post hoc test, *$p < 0.05$, **$p < 0.01$, and ***$p < 0.005$. See also Figure S7.

Error bars indicate SEM.

dendrites remained unaffected by this drug (Figure 6C, right). Following TEA (+ actD + PTX + KYNA) treatment, CPEB3-ir no longer declined in intermediate dendrites, while blocking synaptic transmission and gene transcription (actD + PTX + KYNA) had no effect on the CPEB3-ir gradient (Figure 6D). Thus, the CPEB3 expression level decreases with distance along dendrites, and elevating or reducing Ca^{2+} entry via voltage-gated Ca^{2+} channels can disrupt the CPEB3 gradient. In contrast to CPEB3, the level of peEF2-ir did not change along the dendrites (Δ peEF2-ir/GFP relative to proximal dendrites: 3% ± 11% at 40–60 μm and 8% ± 10% at >60 μm; n = 8). Thus, elevated CPEB3, rather than suppression of protein synthesis by peEF2, leads to a reduction of synaptic GluA2 content at proximal dendrites. Together these data suggest that local changes in CPEB3 distribution may play an important role in establishing or maintaining a GluA2-AMPAR gradient.

We next used an antibody that binds to the extracellular domain of GluA2 to examine the distribution of surface GluA2-ir along the dendrites of cultured stellate cells. Cerebellar neurons were co-immunostained for GluA2 and MAP2 without membrane permeabilization. MAP2, an intracellular protein, was used to detect any permeabilization of the dendrites of GFP-expressing stellate cells, and these dendrites were excluded from further analysis of surface GluA2 expression. Many GluA2-ir puncta were located opposite vGlut puncta (Figure S8A), suggesting that these AMPARs are likely to be activated by presynaptic glutamatergic inputs. We found a higher level of GluA2-ir (total puncta fluoresce = size × fluorescence intensity) at distal dendrites than at proximal dendrites (~50% increase; Figures 6E and 6F) but a lower puncta density at >60 μm (Figure S8C). This spatial change is closely correlated with the increase in RI of EPSCs along dendrites of stellate cells observed in slices (Figure 6F; Figure S8B). Thus, GluA2 expression also increases with dendritic distance in cultured stellate cells.

APs Regulate CPEB3 Expression via a PKC-Dependent Pathway

Blocking AP firing in stellate cells by TTX and attenuation of dendritic AP back-propagation reduce Ca^{2+} entry that occurs through voltage-gated Ca^{2+} channels. Because repetitive Ca^{2+} spikes can activate PKC and PKC detects the pattern of AP firing in sensory neurons (Wan et al., 2012), we tested the idea that Ca^{2+} entry during APs enhances CPEB3 expression in stellate cells by activating PKC.

We first examined whether blocking AP firing in stellate cells suppressed PKC activity. Once PKC is activated, it is translocated to the plasma membrane (Codazzi et al., 2001). We

thus determined the intensity of membrane staining of PKC (active) relative to PKC-ir in the cytoplasm (Figure 7A). As a positive control, we treated the cultures with Phorbol 12-myristate 13-acetate (PMA), a PKC activator, for 30 min, and we found that GFP-positive neurons showed clear membrane staining with little cytoplasmic PKC-ir (Figure 7B). We quantified the distribution of PKC using two methods: first, using line scans across the somata of the GFP-positive neurons to monitor the level of PKC-ir; and second, by quantifying total PKC-ir in the membrane, cytoplasm, and nucleus (Figure 7A).

In control stellate cells incubated with PTX and KYNA, we observed a prominent membrane PKC-ir and cytoplasmic PKC-ir (41% ± 2% versus 37% ± 0.5% of total PKC-ir; 33 cells; Figures 7B and 7C). In contrast, after TTX treatment the level of cytoplasmic PKC-ir increased to 49% ± 3% ($p < 0.02$), while the membrane PKC-ir diminished (26% ± 3%; 33 cells; $p < 0.05$). The $PKC_{membrane}$:$PKC_{cytoplasm}$ ratio decreased from 1.95 ± 0.3 in control to 1.02 ± 0.2 in TTX-treated cells ($p < 0.01$; Figure 7C). When PKC was activated with PMA (0.1 μM) at the end of the TTX treatment, we found that PMA completely abolished the TTX-induced change in PKC-ir (Figures 7B and 7C). To rule out any sampling bias, we calculated the thickness of the membrane staining and found that this was the same in all experimental conditions (Figure S7E). Thus, the reduction in PKC membrane translocation following TTX treatment indicates a decrease in PKC activity.

We next determined whether reducing PKC activity suppressed CPEB3 expression in the soma of stellate cells. Following a 3-hr incubation of cerebellar cultures with the PKC inhibitor chelerythrine (1 μM), we found that the level of somatic CPEB3-ir in GFP-positive neurons decreased by 20% ± 4% (four cultures; RM ANOVA, $p < 0.02$; Figure 7D; Figure S7C). A second PKC inhibitor, bisindolylmaleimide I (0.3 μM), also reduced CPEB3-ir by 18% ± 2% ($p < 0.02$), indicating that PKC activity can regulate CPEB3 expression. If silencing postsynaptic neuronal activity with TTX reduces CPEB3 expression via preventing PKC activation, the presence of a PKC inhibitor during the TTX treatment should not cause a further reduction in CPEB3-ir. Indeed, the reduction in CPEB3-ir following co-incubation of cultures with TTX and chelerythrine was indistinguishable from that after TTX or chelerythrine treatment alone (Figure 7D; Figure S7E). This change (27% ± 2%) was significantly lower than the predicted value if TTX and the PKC inhibitor reduced CPEB3 through two independent (and thus additive) pathways (37% ± 2%; $p < 0.05$). Therefore, TTX treatment occludes the suppression of CPEB3 levels by a PKC inhibitor, suggesting that the PKC-signaling pathway mediates the postsynaptic activity-dependent regulation of CPEB3 expression. This implies that activation of PKC should prevent the TTX-induced decrease in CPEB3. Indeed, in the presence of the PKC activator PMA, TTX failed to reduce CPEB3 expression in stellate cells (Figure 7D; Figure S7G). In contrast to CPEB3 expression, TTX treatment and enhanced or suppressed PKC activity did not alter the GFP signal (Figure S7F). Together these results indicate that blocking somatic APs with TTX reduces the activity of PKC in cerebellar stellate cells, leading to a decrease in CPEB3 expression.

DISCUSSION

Synaptic AMPARs are critical in determining the postsynaptic response, but they are not uniformly distributed on dendrites. A greater number of AMPARs are present at distal compared to proximal dendrites to compensate for dendritic filtering in hippocampal pyramidal neurons (Magee and Cook, 2000; Nicholson et al., 2006; Pettit et al., 1997; Stricker et al., 1996). Synaptic AMPARs of distinct subunit composition are also differentially distributed on spatially segregated dendrites or in an input-specific manner in auditory and hippocampal neurons (Gardner et al., 2001; Tóth and McBain, 1998). Such a gradient of synaptic AMPAR subtypes is predicted to afford the synapse with not only different postsynaptic responses but also distinct forms of synaptic plasticity in a distance-dependent manner, enhancing the computational power of individual neurons. However, the mechanism that controls synaptic strength/properties based on dendritic distance from the soma is not known. Somatic APs actively propagate or passively spread along dendrites, and both dendritic depolarization and Ca^{2+} entry often attenuate with distance (Gasparini and Migliore, 2015; Häusser et al., 2000). This may supply a local dendritic signal to synapses that influence the distribution of synaptic receptors. Here we provide experimental evidence supporting the idea that dendrites not only integrate synaptic signals but also control the spatial distribution of synaptic AMPAR subtypes in a retrograde manner. We identified a CPEB3 expression gradient, which is locally regulated by electrical signals, directly controls GluA2 protein synthesis, and is responsible for the distance-dependent differential expression of synaptic AMPAR subtypes. Our finding that a depolarization-evoked Ca^{2+} rise activates PKC and thus elevates the CPEB3 levels provides a molecular link between electrical signaling and CPEB3 expression. We conclude that sustained AP activity in postsynaptic neurons elevates CPEB3 levels, suppresses GluA2 translation, and promotes GluA2-lacking AMPAR expression at proximal dendrites, establishing a GluA2 gradient along dendrites (Figure S8D).

A GluA2 gradient can give rise to a distance-dependent postsynaptic response to presynaptic input. We have previously shown that incorporation of GluA2 subunits into an AMPAR prolongs the decay time constant of EPSCs and enhances the probability that synaptic inputs evoke APs (Savtchouk and Liu, 2011). Thus, synapses at distal dendrites have a higher rate of excitatory postsynaptic potential (EPSP)-AP coupling. However, GluA2-lacking AMPARs exhibit paired-pulse potentiation due to the release of polyamine block by the second stimulus, and, therefore, proximal synapses would respond more effectively to a train of stimuli, such as those evoked by sensory stimulation (Figure S8E) (Abrahamsson et al., 2012; Chadderton et al., 2004; Savtchouk and Liu, 2011). Furthermore, since GluA2-lacking AMPARs are highly Ca^{2+} permeable and can trigger anti-Hebbian synaptic plasticity, synapses at proximal (but not at distal) dendritic locations can undergo a switch in AMPAR phenotype to GluA2-containing receptors, leading to a reduction in synaptic response (Savtchouk and Liu, 2011). Activation of Ca-permeable AMPARs also can lead to a lasting reduction in glutamate release at parallel fiber to stellate cell synapses (Soler-Llavina and Sabatini, 2006). Thus, a distance-dependent distribution of synaptic

AMPAR subtypes would enable multiple forms of synaptic plasticity to occur, depending on the location of the synapse, and so provide a mechanism for bidirectional synaptic plasticity along dendrites. Indeed, AP back-propagation can influence synaptic plasticity in cortical neurons in a distance-dependent manner (Sjöström and Häusser, 2006).

Although presynaptic activity is known to regulate synaptic AMPARs, it remains poorly understood whether postsynaptic APs influence the composition of synaptic AMPARs. Spontaneous spiking activity has long been recognized as a common feature of many neurons, including olfactory neurons, glutamatergic neurons in the lateral habenula, neostriatal cholinergic interneurons, auditory neurons in the DCN, and GABAergic interneurons in several brain regions (Bennett and Wilson, 1999; Häusser and Clark, 1997; Kowski et al., 2009). While such activity has been implicated in interneuron migration and the establishment of connectivity in the olfactory sensory map (De Marco García et al., 2011; Yu et al., 2004), the function of tonic activity in an established circuit is not well understood. Previous studies have revealed that many of these tonically active neurons also have synaptic GluA2-lacking receptors (Blakemore et al., 2006; Li et al., 2011; Liu and Cull-Candy, 2000; Samoilova et al., 1999). Our results show that loss of tonic activity enhances synaptic GluA2 expression, and they provide evidence supporting the idea that intrinsic activity drives the expression of GluA2-lacking AMPARs. In contrast to spontaneously active neurons, cortical and CA1 pyramidal neurons express a high level of GluA2 mRNA, and postsynaptic activity can suppress GluA2 expression via a transcription-dependent mechanism (Goold and Nicoll, 2010; Ibata et al., 2008). Emerging evidence indicates that experience, such as learning or seizure episodes, can alter intrinsic membrane excitability (Breton and Stuart, 2009; Makara et al., 2009) and convert neurons that are normally silent in the absence of synaptic inputs to ones that display tonic activity (Matthews et al., 2008; Shah et al., 2004). Such a sustained enhancement in the intrinsic activity of postsynaptic neurons may promote the expression of synaptic GluA2-lacking receptors in depolarized dendrites and, thereby, alter the activity of a neuronal network. Indeed, learning and sensory experiences have been shown to increase GluA2-lacking receptors in the amygdala and sensory cortices (Clem and Barth, 2006; Clem and Huganir, 2010; Goel et al., 2006). Thus, our results provide evidence for a role for postsynaptic activity in synaptic homeostasis, which gives rise to a characteristic distance-dependent spatial distribution of synaptic AMPAR subtypes.

We also suggest the local cellular process that converts electrical signals into a spatially confined receptor distribution. CPEB3 protein binds to GluA2 mRNA and regulates GluA2 translation, and it is critical to learning and memory, as mutations in the CPEB3 gene are associated with memory loss (Huang et al., 2006; Theis et al., 2003; Vogler et al., 2009). Thus, an activity-dependent regulation of CPEB3 expression is likely to influence memory formation. We have demonstrated that disruption of the CPEB3-GluA2 mRNA interaction rapidly alters the functional synaptic AMPAR phenotype from GluA2-lacking to GluA2-containing receptors at proximal dendrites, providing direct evidence that the CPEB3-GluA2 interaction suppresses synaptic GluA2 receptors. Intriguingly, we found a CPEB3-ir gradient along dendrites, which appears to closely mimic the GluA2 gradient we report in these cells. However, we are currently limited to using a single, semiquantitative technique (immunocytochemistry) to visualize CPEB3 protein, and, therefore, further confirmation of the gradient-like distribution of CPEB3 needs to be performed once improved tools are available (e.g., with fluorescently tagged endogenous CPEB3 in transgenic mice). We also found that both the CPEB3 and the synaptic GluA2 gradient are disrupted by Ca^{2+} channel blockers. Thus, it is likely that CPEB3 in dendrites controls the local synthesis of GluA2 and the content of synaptic GluA2.

Our finding that membrane depolarization elevates CPEB3 levels suggests that somatic APs act as a centrifugal signal that controls the dendritic synthesis and expression of synaptic receptors. The dendritic GluA2-ir that was located near the soma (<14 μm) appeared to be higher than in the proximal region (14–40 μm), and this is consistent with a greater RI of the EPSCs in this dendritic region (Figure S1A). The expression of somatic receptors is controlled by a different regulatory protein(s) than synaptic AMPARs (Bats et al., 2012), and it may undergo a distinct form of activity-dependent regulation. Consistent with the idea of an activity-dependent increase in CPEB3, seizure activity increases the expression of CPEB3 mRNA in hippocampal pyramidal cells that normally express low levels of CPEB3 (Theis et al., 2003). This, however, contrasts with an NMDAR-triggered downregulation of CPEB3 levels via calpain-dependent protein degradation (Wang and Huang, 2012), suggesting that somatic APs and synaptic activity may produce two opposing effects on CPEB3 levels. A recent study showed that spatial learning promotes mono-ubiquitination of CPEB3 by Neutralized1 and enhances the expression of GluA2 and 1. (Pavlopoulos et al., 2011). Thus, neuronal activity alters synaptic AMPAR subtype and number by two distinct mechanisms, namely, regulation of the expression and the activity of CPEB3, respectively.

We found that postsynaptic APs activate PKC, and tonic PKC activity is critical for elevating and maintaining the CPEB3 levels that suppress GluA2 expression in stellate cells. This is a novel cell-autonomous plasticity mechanism by which the basal activity of a postsynaptic cell controls the expression of its own GluA2 receptors. Such a mechanism does not rely on synaptic input or changes in gene transcription, and, thus, it fundamentally differs from the regulation of synaptic AMPAR phenotype by presynaptic activity and neuromodulators in response to external stimuli. However, the interplay between the cell-autonomous and input-dependent types of plasticity is yet to be explored. For example, we have shown previously that noradrenaline release during acute stress enhances GluA2 gene transcription and, thus, synaptic GluA2 expression in stellate cells (Liu et al., 2010). Overwhelming evidence indicates that glutamate secretion from presynaptic terminals can alter postsynaptic AMPARs via PICK1-dependent recycling of GluA2 and protein synthesis-dependent pathways. The latter commonly involves the regulation of activity-regulated cytoskeleton-associated proteins and CaMKII by fragile X mental retardation protein, which alters receptor trafficking (Bear et al., 2004; Gardner et al., 2005; Kelly et al., 2009; Liu and Cull-Candy, 2005; Lüscher and Huber, 2010; Sun and June Liu, 2007; Sutton and Schuman, 2006). In contrast, postsynaptic firing directly regulates CPEB3 levels

and GluA2 translation, a mechanism that is distinct from the regulation of receptor trafficking and transcription. The possibility that somatic APs also may regulate AMPAR trafficking remains to be tested. While presynaptic activity promotes GluA2 expression, somatic APs reduce the synaptic GluA2 content. Thus, these two processes are regulated by two distinct physiological signals, produce two opposite synaptic phenotypes, and utilize two different mechanisms. Suppression of GluA2 protein synthesis by somatic APs may provide a mechanism to reverse the synaptic activity-induced increase in GluA2 levels.

Our results show that changes in synaptic AMPAR subtypes occur within a few hours following the disruption of GluA2 mRNA-CPEB3 interactions and pharmacological inhibition of protein synthesis. This process is slower than the synaptic activity-induced plasticity via AMPAR trafficking, but it is faster than the overall AMPAR turnover and endocytosis rate, which range from hours to days (Cohen et al., 2013; Ehlers, 2000). Since several AMPAR pools with different turnover rates contribute to the overall AMPAR maintenance, one possibility is that dendritic GluA2 synthesis represents a pool that is regulated by postsynaptic APs and enables a more rapid cycling rate of GluA2 at dendritic sites (Cohen et al., 2013). A gradient of CPEB3 proteins along dendrites enables both the spatial and subunit specificity of dendritic AMPAR distribution, although the overall turnover and endocytosis rate are not different among AMPAR subunits (Cohen et al., 2013; Ehlers, 2000).

Dendritic gradients have emerged as a common feature of neurons in the CNS. In addition to synaptic receptors, the density of voltage-gated ion channels also changes with dendritic distance (Hoffman et al., 1997; Kole et al., 2006; Magee, 1998; Nörenberg et al., 2010; Sjöström and Häusser, 2006). Our experiments indicate the existence of a cell-autonomous mechanism in which retrograde APs control dendritic CPEB3 levels and, thereby, synaptic AMPAR subunit expression. These results highlight the importance of local synthesis of synaptic receptors as a way to establish a spatially graded expression pattern. We conclude that postsynaptic AP firing sets up the dendritic gradient of synaptic AMPAR subtypes and serves as a powerful means to control excitatory drive and the response to incoming synaptic signals. A dendritic GluA2 gradient would preferentially amplify proximal synaptic inputs and enable these synapses to undergo anti-Hebbian synaptic plasticity to reduce synaptic drive. Such a spatially defined synaptic response and plasticity at the parallel fiber-stellate cell synapse may enhance the ability of cerebellar circuitry to process sensory information and experience-dependent learning. Given the importance of activity-dependent change in AMPAR phenotype, for example, in learning and in the neuronal death that is associated with various neurological disorders (reviewed in Liu and Zukin, 2007), a postsynaptic AP-driven synaptic plasticity would present a novel mechanism for a modification of AMPAR subtypes in dendrites.

EXPERIMENTAL PROCEDURES

Complete details of experimental conditions, methods, and analysis are provided in the Supplemental Experimental Procedures. Experimental procedures were in accordance with the Louisiana State University Health Sciences Center and Penn State University guidelines for care and use of laboratory animals (IACUC).

Slice Preparation and Incubation

C57/BL6 mice (P18–23) were decapitated in accordance with the animal welfare guidelines of Louisiana State University (LSU) Health Sciences Center (HSC) and Penn State University. Cerebellar slices were prepared as described previously (Liu et al., 2010; Savtchouk and Liu, 2011). Following decapitation, cerebellar slices (250–300 μm) were obtained with a Leica VT1200 vibrating microslicer. Cerebellar dissection and slicing were performed in an ice-cold slicing solution (in mM: 125 NaCl, 2.5 KCl, 0.5 $CaCl_2$, 7 $MgCl_2$, 26 $NaHCO_3$, 1.25 NaH_2PO_4, and 25 glucose, saturated with 95% O_2-5% CO_2 [pH 7.4]). Slices were maintained in external ACSF (in mM: 125 NaCl, 2.5 KCl, 2 $CaCl_2$, 1 $MgCl_2$, 26 $NaHCO_3$, 1.25 NaH_2PO_4, and 25 glucose) at room temperature. In several experiments, cerebellar slices were incubated in ACSF containing 1 mM KYNA and 0.1 mM PTX (as control) or with the addition of drugs for at least 3 hr before recording.

Electrophysiology

Whole-cell patch-clamp recordings were obtained using an Axoclamp 700A or 700B amplifier (Axon Instruments). Stellate cells located in the outer two-thirds of the molecular layer were visually identified under differential interference contrast (DIC) using a 60× upright water-immersion objective and by the presence of APs in the cell-attached configuration and spontaneous synaptic currents in the whole-cell configuration, as described previously (Liu and Cull-Candy, 2000). Whole-cell recordings were performed using 5–7 MΩ borosilicate glass pipettes, and the cell series resistance was monitored throughout the experiment. The recording was terminated if the series resistance changed by more than 20%–30%. All recordings were performed at room temperature.

Evoked EPSCs

Voltage-clamp recordings were performed in sagittal slices using a cesium-based internal solution (in mM: 135 CsCl, 10 EGTA-Cs, 10 HEPES, 4 ATP-Na, 4 MgCl2, 5 TEA, and 1 QX314 [pH adjusted to 7.3]). To determine the subunit composition of synaptic AMPARs, 100 μM spermine was included in the internal solution unless otherwise indicated. Spermine and endogenous polyamines block GluA2-lacking (but not GluA2-containing) AMPARs at positive potentials. Therefore, synaptic GluA2 content at a synapse was assessed by comparing the synaptic conductance at positive and negative potentials from the I-V relationship. Synaptic AMPAR currents were evoked by placing a monopolar glass stimulating electrode filled with ACSF at various distances from the soma of a patched cell and applying brief (~400-μs) voltage pulses (5–25 V), in the presence of 200 μM PTX and 10 μM R-CPP at 0.3 Hz to block GABA and NMDA receptors, respectively. The stimulation strength was adjusted such that 50% of stimuli evoked EPSCs to minimize stimulation of multiple synapses.

To achieve a local, targeted activation of the parallel fibers, we used a stimulation pipette with a small opening (5–8 MΩ), ejecting minimal currents to achieve threshold stimulation (50% failure rate).

Dendritic Distance Measurements

In a few pilot experiments, we included 20 μM Alexa Fluor 488 in the pipette solution to visualize the dendritic processes and more accurately measure the synaptic distance. However, Alexa 488, when included in the pipette solution, alters the RI of EPSCs (Figure S1C), and, therefore, it was not used to reveal dendritic morphology in electrophysiology experiments. We therefore estimated the dendritic length by the Cartesian distance between recording and stimulating electrodes.

CPEB3 Oligonucleotide (Aptamer) Experiments

To examine whether CPEB3 was involved in the synaptic GluA2 gradient, we used a synthetic RNA oligonucleotide sequence previously shown to disrupt the interaction of GluA2 mRNA and CPEB3 (Huang et al., 2006).

Ca^{2+} Imaging

For Ca^{2+}-imaging experiments (Gasparini, 2011), whole-cell patch-clamp somatic recordings were performed using a Dagan BVC-700 amplifier in the active bridge mode. Trains of five somatic APs at 100 Hz were elicited by the injection of brief current steps (300–600 pA, 2-ms duration each). Patch pipettes were filled with a solution containing (in mM): 130 K-methylsulphonate,

10 HEPES, 4 NaCl, 4 Mg_2ATP, 0.3 $Tris_2GTP$, 14 phosphocreatine, and 0.1 Oregon Green BAPTA-1 (OGB-1) hexapotassium salt; the resistance of the electrodes was 4–6 MΩ. OGB-1 was excited using a Chameleon Ultra laser (Coherent) emitting ultra-fast, pulsed light at 920 nm; the emitted fluorescence was detected using an Ultima scanner (Prairie Technologies) mounted over an Olympus BX61WI microscope.

Primary Cerebellar Cell Culture

Cerebellar cell cultures were prepared using P7 wild-type and mutant mouse pups expressing EGFP under the GAD65 (GAD65::GFP) or GAD67 promoter (GAD67::GFP; from the Jackson Laboratory). Cells were maintained for 18–27 days in vitro at 37°C in 5% CO_2. Stellate cells were visually identified by GFP expression.

Immunocytochemistry

Cultured cerebellar neurons were washed in PBS and fixed in 4% paraformaldehyde in PBS for 20 min. A full list of antibodies, staining conditions, and image acquisition and analysis are provided in the Supplemental Experimental Procedures.

Statistics

All values are expressed as mean ± SEM. Statistical significance was assessed using ANOVA, RM ANOVA, or Student's t tests (paired, unpaired two-tailed, or one sample), as appropriate if a dataset passed the Shapiro-Wilk normality test. Otherwise, Mann-Whitney test and Wilcoxon signed-rank test were used. The Kolmogorov-Smirnov test was used for comparison of cumulative distribution plots. A summary of the statistical analysis is shown in Table S1.

SUPPLEMENTAL INFORMATION

Supplemental Information includes Supplemental Experimental Procedures, eight figures, and one table and can be found with this article online at http://dx.doi.org/10.1016/j.celrep.2016.08.094.

AUTHOR CONTRIBUTIONS

I.S., L.S., C.L.B., Q.Y., S.G. and S.J.L. designed and performed the experiments and analyzed the data. G.S. generated GAD65::GFP mice. I.S., C.L.B., S.G. and S.J.L. wrote the manuscript. S.J.L. conceived and designed the study.

ACKNOWLEDGMENTS

This work was supported by National Science Foundation Grant IBN-0344559 and NIH Grants NS58867 and MH095948 (S.J.L.) and NS069714 (S.G.). We thank Drs. Kathryn L. Carzoli, Christophe J. Dubois, Matthieu Maroteaux, Yu Liu, Charles Nichols, and Matthew Whim for experimental advice and helpful discussions and the LSU HSC Neuroscience COBRE multi photon core (P30-GM103340).

Received: September 10, 2014
Revised: July 13, 2016
Accepted: August 29, 2016
Published: September 27, 2016

REFERENCES

Abrahamsson, T., Cathala, L., Matsui, K., Shigemoto, R., and Digregorio, D.A. (2012). Thin dendrites of cerebellar interneurons confer sublinear synaptic integration and a gradient of short-term plasticity. Neuron *73*, 1159–1172.

Bats, C., Soto, D., Studniarczyk, D., Farrant, M., and Cull-Candy, S.G. (2012). Channel properties reveal differential expression of TARPed and TARPless AMPARs in stargazer neurons. Nat. Neurosci. *15*, 853–861.

Bear, M.F., Huber, K.M., and Warren, S.T. (2004). The mGluR theory of fragile X mental retardation. Trends Neurosci. *27*, 370–377.

Benke, T.A., Lüthi, A., Isaac, J.T., and Collingridge, G.L. (1998). Modulation of AMPA receptor unitary conductance by synaptic activity. Nature *393*, 793–797.

Bennett, B.D., and Wilson, C.J. (1999). Spontaneous activity of neostriatal cholinergic interneurons in vitro. J. Neurosci. *19*, 5586–5596.

Blakemore, L.J., Resasco, M., Mercado, M.A., and Trombley, P.Q. (2006). Evidence for Ca(2+)-permeable AMPA receptors in the olfactory bulb. Am. J. Physiol. Cell Physiol. *290*, C925–C935.

Bowie, D., and Mayer, M.L. (1995). Inward rectification of both AMPA and kainate subtype glutamate receptors generated by polyamine-mediated ion channel block. Neuron *15*, 453–462.

Breton, J.D., and Stuart, G.J. (2009). Loss of sensory input increases the intrinsic excitability of layer 5 pyramidal neurons in rat barrel cortex. J. Physiol. *587*, 5107–5119.

Chadderton, P., Margrie, T.W., and Häusser, M. (2004). Integration of quanta in cerebellar granule cells during sensory processing. Nature *428*, 856–860.

Clem, R.L., and Barth, A. (2006). Pathway-specific trafficking of native AMPARs by in vivo experience. Neuron *49*, 663–670.

Clem, R.L., and Huganir, R.L. (2010). Calcium-permeable AMPA receptor dynamics mediate fear memory erasure. Science *330*, 1108–1112.

Codazzi, F., Teruel, M.N., and Meyer, T. (2001). Control of astrocyte Ca(2+) oscillations and waves by oscillating translocation and activation of protein kinase C. Curr. Biol. *11*, 1089–1097.

Cohen, L.D., Zuchman, R., Sorokina, O., Müller, A., Dieterich, D.C., Armstrong, J.D., Ziv, T., and Ziv, N.E. (2013). Metabolic turnover of synaptic proteins: kinetics, interdependencies and implications for synaptic maintenance. PLoS ONE *8*, e63191.

Cull-Candy, S., Kelly, L., and Farrant, M. (2006). Regulation of Ca2+-permeable AMPA receptors: synaptic plasticity and beyond. Curr. Opin. Neurobiol. *16*, 288–297.

De Marco García, N.V., Karayannis, T., and Fishell, G. (2011). Neuronal activity is required for the development of specific cortical interneuron subtypes. Nature *472*, 351–355.

Ehlers, M.D. (2000). Reinsertion or degradation of AMPA receptors determined by activity-dependent endocytic sorting. Neuron *28*, 511–525.

Gardner, S.M., Trussell, L.O., and Oertel, D. (2001). Correlation of AMPA receptor subunit composition with synaptic input in the mammalian cochlear nuclei. J. Neurosci. *21*, 7428–7437.

Gardner, S.M., Takamiya, K., Xia, J., Suh, J.G., Johnson, R., Yu, S., and Huganir, R.L. (2005). Calcium-permeable AMPA receptor plasticity is mediated by subunit-specific interactions with PICK1 and NSF. Neuron *45*, 903–915.

Gasparini, S. (2011). Distance- and activity-dependent modulation of spike back-propagation in layer V pyramidal neurons of the medial entorhinal cortex. J. Neurophysiol. *105*, 1372–1379.

Gasparini, S., and Migliore, M. (2015). Action Potential Backpropagation. In Encyclopedia of Computational Neuroscience, D. Jaeger and R. Jung, eds. (New York, NY: Springer New York), pp. 133–137.

Goel, A., Jiang, B., Xu, L.W., Song, L., Kirkwood, A., and Lee, H.K. (2006). Cross-modal regulation of synaptic AMPA receptors in primary sensory cortices by visual experience. Nat. Neurosci. *9*, 1001–1003.

Goold, C.P., and Nicoll, R.A. (2010). Single-cell optogenetic excitation drives homeostatic synaptic depression. Neuron *68*, 512–528.

Häusser, M., and Clark, B.A. (1997). Tonic synaptic inhibition modulates neuronal output pattern and spatiotemporal synaptic integration. Neuron *19*, 665–678.

Häusser, M., Spruston, N., and Stuart, G.J. (2000). Diversity and dynamics of dendritic signaling. Science *290*, 739–744.

Helmchen, F. (2007). Biochemical compartmentalization in dendrites. In Dendrites, G. Stuart, Nelson Spruston, and Michael Häusser, Second Edition, G. Stuart, N. Spruston, and M. Häusser, eds. (Oxford: Oxford University Press).

Hoffman, D.A., Magee, J.C., Colbert, C.M., and Johnston, D. (1997). K+ channel regulation of signal propagation in dendrites of hippocampal pyramidal neurons. Nature *387*, 869–875.

Huang, Y.S., Kan, M.C., Lin, C.L., and Richter, J.D. (2006). CPEB3 and CPEB4 in neurons: analysis of RNA-binding specificity and translational control of AMPA receptor GluR2 mRNA. EMBO J. *25*, 4865–4876.

Ibata, K., Sun, Q., and Turrigiano, G.G. (2008). Rapid synaptic scaling induced by changes in postsynaptic firing. Neuron *57*, 819–826.

Kamboj, S.K., Swanson, G.T., and Cull-Candy, S.G. (1995). Intracellular spermine confers rectification on rat calcium-permeable AMPA and kainate receptors. J. Physiol. *486*, 297–303.

Kelly, L., Farrant, M., and Cull-Candy, S.G. (2009). Synaptic mGluR activation drives plasticity of calcium-permeable AMPA receptors. Nat. Neurosci. *12*, 593–601.

Kole, M.H., Hallermann, S., and Stuart, G.J. (2006). Single Ih channels in pyramidal neuron dendrites: properties, distribution, and impact on action potential output. J. Neurosci. *26*, 1677–1687.

Kowski, A.B., Veh, R.W., and Weiss, T. (2009). Dopaminergic activation excites rat lateral habenular neurons in vivo. Neuroscience *161*, 1154–1165.

Li, B., Piriz, J., Mirrione, M., Chung, C., Proulx, C.D., Schulz, D., Henn, F., and Malinow, R. (2011). Synaptic potentiation onto habenula neurons in the learned helplessness model of depression. Nature *470*, 535–539.

Liu, S.Q., and Cull-Candy, S.G. (2000). Synaptic activity at calcium-permeable AMPA receptors induces a switch in receptor subtype. Nature *405*, 454–458.

Liu, S.J., and Cull-Candy, S.G. (2002). Activity-dependent change in AMPA receptor properties in cerebellar stellate cells. J. Neurosci. *22*, 3881–3889.

Liu, S.J., and Cull-Candy, S.G. (2005). Subunit interaction with PICK and GRIP controls Ca2+ permeability of AMPARs at cerebellar synapses. Nat. Neurosci. *8*, 768–775.

Liu, S.J., and Zukin, R.S. (2007). Ca2+-permeable AMPA receptors in synaptic plasticity and neuronal death. Trends Neurosci. *30*, 126–134.

Liu, S., Lau, L., Wei, J., Zhu, D., Zou, S., Sun, H.S., Fu, Y., Liu, F., and Lu, Y. (2004). Expression of Ca(2+)-permeable AMPA receptor channels primes cell death in transient forebrain ischemia. Neuron *43*, 43–55.

Liu, Y., Formisano, L., Savtchouk, I., Takayasu, Y., Szabó, G., Zukin, R.S., and Liu, S.J. (2010). A single fear-inducing stimulus induces a transcription-dependent switch in synaptic AMPAR phenotype. Nat. Neurosci. *13*, 223–231.

Liu, Y., Savtchouk, I., Acharjee, S., and Liu, S.J. (2011). Inhibition of Ca2+-activated large-conductance K+ channel activity alters synaptic AMPA receptor phenotype in mouse cerebellar stellate cells. J. Neurophysiol. *106*, 144–152.

Lüscher, C., and Huber, K.M. (2010). Group 1 mGluR-dependent synaptic long-term depression: mechanisms and implications for circuitry and disease. Neuron *65*, 445–459.

Magee, J.C. (1998). Dendritic hyperpolarization-activated currents modify the integrative properties of hippocampal CA1 pyramidal neurons. J. Neurosci. *18*, 7613–7624.

Magee, J.C., and Cook, E.P. (2000). Somatic EPSP amplitude is independent of synapse location in hippocampal pyramidal neurons. Nat. Neurosci. *3*, 895–903.

Magee, J.C., and Johnston, D. (2005). Plasticity of dendritic function. Curr. Opin. Neurobiol. *15*, 334–342.

Major, G., Polsky, A., Denk, W., Schiller, J., and Tank, D.W. (2008). Spatiotemporally graded NMDA spike/plateau potentials in basal dendrites of neocortical pyramidal neurons. J. Neurophysiol. *99*, 2584–2601.

Makara, J.K., Losonczy, A., Wen, Q., and Magee, J.C. (2009). Experience-dependent compartmentalized dendritic plasticity in rat hippocampal CA1 pyramidal neurons. Nat. Neurosci. *12*, 1485–1487.

Maroteaux, M., and Mameli, M. (2012). Cocaine evokes projection-specific synaptic plasticity of lateral habenula neurons. J. Neurosci. *32*, 12641–12646.

Matthews, E.A., Weible, A.P., Shah, S., and Disterhoft, J.F. (2008). The BK-mediated fAHP is modulated by learning a hippocampus-dependent task. Proc. Natl. Acad. Sci. USA *105*, 15154–15159.

Menuz, K., Stroud, R.M., Nicoll, R.A., and Hays, F.A. (2007). TARP auxiliary subunits switch AMPA receptor antagonists into partial agonists. Science *318*, 815–817.

Myoga, M.H., Beierlein, M., and Regehr, W.G. (2009). Somatic spikes regulate dendritic signaling in small neurons in the absence of backpropagating action potentials. J. Neurosci. *29*, 7803–7814.

Nicholson, D.A., Trana, R., Katz, Y., Kath, W.L., Spruston, N., and Geinisman, Y. (2006). Distance-dependent differences in synapse number and AMPA receptor expression in hippocampal CA1 pyramidal neurons. Neuron *50*, 431–442.

Noh, K.M., Yokota, H., Mashiko, T., Castillo, P.E., Zukin, R.S., and Bennett, M.V. (2005). Blockade of calcium-permeable AMPA receptors protects hippocampal neurons against global ischemia-induced death. Proc. Natl. Acad. Sci. USA *102*, 12230–12235.

Nörenberg, A., Hu, H., Vida, I., Bartos, M., and Jonas, P. (2010). Distinct nonuniform cable properties optimize rapid and efficient activation of fast-spiking GABAergic interneurons. Proc. Natl. Acad. Sci. USA *107*, 894–899.

Pavlopoulos, E., Trifilieff, P., Chevaleyre, V., Fioriti, L., Zairis, S., Pagano, A., Malleret, G., and Kandel, E.R. (2011). Neuralized1 activates CPEB3: a function for nonproteolytic ubiquitin in synaptic plasticity and memory storage. Cell *147*, 1369–1383.

Pettit, D.L., Wang, S.S., Gee, K.R., and Augustine, G.J. (1997). Chemical two-photon uncaging: a novel approach to mapping glutamate receptors. Neuron *19*, 465–471.

Rozov, N., and Burnashev, N. (1999). Polyamine-dependent facilitation of postsynaptic AMPA receptors counteracts paired-pulse depression. Nature *401*, 594–598.

Samoilova, M.V., Buldakova, S.L., Vorobjev, V.S., Sharonova, I.N., and Magazanik, L.G. (1999). The open channel blocking drug, IEM-1460, reveals functionally distinct alpha-amino-3-hydroxy-5-methyl-4-isoxazolepropionate receptors in rat brain neurons. Neuroscience *94*, 261–268.

Savtchouk, I., and Liu, S.J. (2011). Remodeling of synaptic AMPA receptor subtype alters the probability and pattern of action potential firing. J. Neurosci. *31*, 501–511.

Shah, M.M., Anderson, A.E., Leung, V., Lin, X., and Johnston, D. (2004). Seizure-induced plasticity of h channels in entorhinal cortical layer III pyramidal neurons. Neuron *44*, 495–508.

Sjöström, P.J., and Häusser, M. (2006). A cooperative switch determines the sign of synaptic plasticity in distal dendrites of neocortical pyramidal neurons. Neuron *51*, 227–238.

Soler-Llavina, G.J., and Sabatini, B.L. (2006). Synapse-specific plasticity and compartmentalized signaling in cerebellar stellate cells. Nat. Neurosci. *9*, 798–806.

Soto, D., Coombs, I.D., Kelly, L., Farrant, M., and Cull-Candy, S.G. (2007). Stargazin attenuates intracellular polyamine block of calcium-permeable AMPA receptors. Nat. Neurosci. *10*, 1260–1267.

Stricker, C., Field, A.C., and Redman, S.J. (1996). Statistical analysis of amplitude fluctuations in EPSCs evoked in rat CA1 pyramidal neurones in vitro. J. Physiol. *490*, 419–441.

Sun, L., and June Liu, S. (2007). Activation of extrasynaptic NMDA receptors induces a PKC-dependent switch in AMPA receptor subtypes in mouse cerebellar stellate cells. J. Physiol. *583*, 537–553.

Sutton, M.A., and Schuman, E.M. (2006). Dendritic protein synthesis, synaptic plasticity, and memory. Cell *127*, 49–58.

Sutton, M.A., Taylor, A.M., Ito, H.T., Pham, A., and Schuman, E.M. (2007). Postsynaptic decoding of neural activity: eEF2 as a biochemical sensor coupling miniature synaptic transmission to local protein synthesis. Neuron *55*, 648–661.

Tharani, Y., Thurlow, G.A., and Turner, R.W. (1996). Distribution of omega-Conotoxin GVIA binding sites in teleost cerebellar and electrosensory neurons. J. Comp. Neurol. *364*, 456–472.

Theis, M., Si, K., and Kandel, E.R. (2003). Two previously undescribed members of the mouse CPEB family of genes and their inducible expression in

the principal cell layers of the hippocampus. Proc. Natl. Acad. Sci. USA *100*, 9602–9607.

Tóth, K., and McBain, C.J. (1998). Afferent-specific innervation of two distinct AMPA receptor subtypes on single hippocampal interneurons. Nat. Neurosci. *1*, 572–578.

Traynelis, S.F., Silver, R.A., and Cull-Candy, S.G. (1993). Estimated conductance of glutamate receptor channels activated during EPSCs at the cerebellar mossy fiber-granule cell synapse. Neuron *11*, 279–289.

Vogler, C., Spalek, K., Aerni, A., Demougin, P., Müller, A., Huynh, K.D., Papassotiropoulos, A., and de Quervain, D.J. (2009). CPEB3 is associated with human episodic memory. Front. Behav. Neurosci. *3*, 4.

Wan, Q., Jiang, X.Y., Negroiu, A.M., Lu, S.G., McKay, K.S., and Abrams, T.W. (2012). Protein kinase C acts as a molecular detector of firing patterns to mediate sensory gating in Aplysia. Nat. Neurosci. *15*, 1144–1152.

Wang, C.F., and Huang, Y.S. (2012). Calpain 2 activated through N-methyl-D-aspartic acid receptor signaling cleaves CPEB3 and abrogates CPEB3-repressed translation in neurons. Mol. Cell. Biol. *32*, 3321–3332.

Yu, C.R., Power, J., Barnea, G., O'Donnell, S., Brown, H.E., Osborne, J., Axel, R., and Gogos, J.A. (2004). Spontaneous neural activity is required for the establishment and maintenance of the olfactory sensory map. Neuron *42*, 553–566.